MECHANICAL AND CHEMICAL PROPERTIES OF NANOPARTICLE-COATED E-GLASS FIBERS FOR COMPOSITES APPLICATIONS

A THESIS SUBMITTED TO

THE GRADUATE SCHOOL OF ENGINEERING AND SCIENCE

OF BILKENT UNIVERSITY

IN PARTIAL FULFILLMENT OF THE REQUIREMENTS FOR

THE DEGREE OF

MASTER OF SCIENCE

IN

MATERIALS SCIENCE AND NANOTECHNOLOGY

By

Md Kawsar Ahmed

July 2023

MECHANICAL AND CHEMICAL PROPERTIES OF NANOPARTICLE-COATED E-GLASS FIBERS FOR COMPOSITES APPLICATIONS

By Md Kawsar Ahmed

July 2023

We certify that we have read this thesis and that in our opinion it is fully adequate, in scope and in quality, as a thesis for the degree of Master of Science.

Engin Durgun(Advisor)

Mustafa Ordu(Co-Advisor)

Mehmet Yılmaz

Hüsnü Emrah Ünalan

Approved for the Graduate School of Engineering and Science:

Orhan Arıkan
Director of the Graduate School

ABSTRACT

MECHANICAL AND CHEMICAL PROPERTIES OF NANOPARTICLE-COATED E-GLASS FIBERS FOR COMPOSITES APPLICATIONS

Md Kawsar Ahmed
M.S. in Materials Science and Nanotechnology
Advisor: Engin Durgun
Co-Advisor: Mustafa Ordu
July 2023

Glass fibers are the most extensively employed reinforcement materials in the fiber-reinforced composites field owing to their superior mechanical properties with cost-effectiveness. The mechanical and chemical properties of the composites are greatly dependent upon the reinforcement materials. In order to enhance the performance of composites, it is necessary to improve the mechanical property of the reinforcement materials, i.e., glass fibers. In this thesis, the mechanical and chemical properties of E-glass fibers were investigated via the incorporation of metal oxide nanoparticles. As part of this process, E-glass fibers were dip-coated with nanoparticle solutions using titania (TiO_2), silica (SiO_2), and zirconia (ZrO_2) nanoparticles. Microscopic and spectroscopic analysis proved the presence of nanoparticles on the surface of the fibers. Tensile tests were conducted on bare and nanoparticle-coated fibers to see the effect of coating and the concentration of nanoparticles over the fiber's surface. Weibull statistical analysis was carried out on bare and coated fibers to see the effect of stress on the probability of failures of the E-glass fibers. A fractographic study was also carried out on E-glass fibers to see the effect of tensile strength on the mirror region of the fracture surface. Additionally, chemical analysis was also carried out to see the resistivity of the fibers in a highly alkaline environment. The results suggest that glass fibers coated with TiO_2 nanoparticles improved the tensile strength of fibers up to 11.7% by providing a lower probability of failure. On the other hand, coating with SiO_2 nanoparticles had a slightly negative impact on the strength of fibers due to the lower quality of coating, leading to a decrease in the tensile strength and an increase in the probability of failure. Moreover, ZrO_2 nanoparticles were found effective in providing resistance against the corrosion to the glass fibers in an alkaline environment for up to 4 days of dwelling. Nanoparticle-coated E-glass

fibers are expected to improve the mechanical and chemical properties of glass fiber-reinforced composites for various industrial applications in the future.

Keywords: Glass fibers, Weibull distribution, Mechanical properties, Alkaline resistance, Fractography, Composites..

ÖZET

KOMPOZIT UYGULAMALARI IÇIN NANOPARÇACIK KAPLAMALI E-CAM ELYAFLARIN MEKANIK VE KIMYASAL ÖZELLIKLERI

Md Kawsar Ahmed
Malzeme Bilimi ve Nanoteknoloji, Yüksek Lisans
Tez Danışmanı: Engin Durgun
İkinci Tez Danışmanı: Mustafa Ordu
Temmuz 2023

Cam elyaflar, üstün mekanik özellikleri ve maliyet etkinliği nedeniyle elyaf-kompozit alanında en yaygın kullanılan takviye malzemelerdir. Kompozitlerin mekanik ve kimyasal özellikleri büyük ölçüde takviye malzemelerine bağlıdır. Kompozitlerin performansını artırmak için cam elyaf gibi takviye malzemelerin mekanik özelliklerinin iyileştirilmesi gerekmektedir. Bu tezde, E-cam elyafların mekanik ve kimyasal özellikleri, elyafların metal oksit nanoparçacıklar ile kaplanmasından sonra incelenmiştir. Bu işlemin bir parçası olarak, E-cam elyaflar titanya (TiO_2), silika (SiO_2) ve zirkonya (ZrO_2) nanoparçacıkları kullanılarak hazırlanmış nanoparçacık çözeltilerine daldırıldı ve kaplama işlemi gerçekleştirildi. Mikroskobik ve spektroskopik analizler sayesinde elyafların yüzeyinde nanopartiküllerin varlığı kanıtladı. Kaplamanın etkisini ve elyaf yüzeyi üzerindeki nanoparçacıkların konsantrasyonunu görmek için çıplak (hiçbir yüzey kaplaması olmayan) ve nanoparçacık kaplı elyaflar üzerinde çekme testleri yapılmıştır. Weibull istatistiksel analizi, stresin E-cam elyaflarının bozulma olasılığı üzerindeki etkisini görmek için çıplak ve kaplanmış elyaflar üzerinde gerçekleştirilmiştir. Çekme mukavemetinin elyaf yüzeyinin ayna bölgesi üzerindeki etkisini görmek için E-cam elyafları üzerinde fraktografik bir çalışma da yapılmıştır. Ek olarak, yüksek alkali ortamda elyafların özdirencini görmek için kimyasal analiz de yapılmıştır. Sonuçlar, TiO_2 nanoparçacıkları ile kaplanmış cam elyafların, daha düşük bir kırılma olasılığı sağlayarak elyafların gerilme mukavemetini % 11,7'ye kadar iyileştirdiğini göstermektedir. Öte yandan, SiO_2 nanoparçacıklar ile kaplamanın, kaplama kalitesinin düşük olması nedeniyle elyafların mukavemeti üzerinde biraz olumsuz etkisi olmuş, bu da çekme mukavemetinde bir düşüşe ve başarısızlık olasılığında artışa yol açmıştır. Ayrıca, ZrO_2 nanoparçacıklarının

alkali ortamda 4 güne kadar kalarak cam elyafların korozyona karşı direnç sağlamasında etkili olduğu görülmüştür. Nanoparçacık kaplı E-cam elyafların gelecekte çeşitli endüstriyel uygulamalar için cam elyaf takviyeli kompozitlerin mekanik ve kimyasal özelliklerini iyileştirmesi beklenmektedir.

Anahtar sözcükler: Cam elyaf, Weibull dağılımı, Mekanik özellikler, Alkalin direnci, Fraktografi, Kompozitler. .

Acknowledgement

Many people have contributed to the completion of my MS at Bilkent University. First and foremost, I would like to sincerely thank my advisor Dr. Mustafa Ordu for accepting me as a graduate student and allowing me to work in his research group. I would also like to thank him for his continuous support, supervision, and constructive criticism in this work.

Secondly, I would like to thank the jury members of my thesis committee, Dr. Engin Durgun, Dr. Mehmet Yılmaz, and Dr. Hüsnü Emrah Ünalan, for finding their valuable time to evaluate my thesis and feedback.

I would also like to thank past and present members of "Contemporary Fibers Laboratory," who were always welcoming and friendly towards me. I especially want to thank Ali Bagheri Behboud and Arda Kurucu for helping me with the experimental work. I would also like to thank SISECAM Inc, and specially Dr. Göksenin Çömlekçi for fabricating the glass fibers and, providing us necessary chemicals. I would also like to thank Papon, Sazid, Rasha, Dhrubo, Faysal, Zain, Dalia, Momil, Faruk, Asfand, Ashfaq, Rummon, Reham, Muzaffar, Robab, Yusuf, and Dilan for their friendship which allowed me to feel at home in a different country. My life at Bilkent University was enjoyable because of them. I would also like to take this opportunity to thank UNAM facilities for providing me with all the equipment and training required for conducting my experimental work. I have asked for countless help from Mr. Semih Bozkurt for the SEM.

I would also like to especially thank the people working in Dormitory 75 for making me feel at home. I would like to thank Ilkay Hanim, Dilek Hanim, Merve, Emine Hanim, Yeter Abla, and Hacer Abla for making this dormitory a second home for me. If I look back at my stay at Türkiye, I would remember these people in my life.

Above all, I would like to thank my mother, father, and sisters for encouraging me, giving me confidence, standing beside me, and holding me back whenever I

needed them. Whatever I have become in my life would be impossible without my family. My dear family, I love you! ...

Dedicated to my mother, father, and sisters.

Contents

List of Figures

List of Tables

Chapter 1

Introduction

1.1 Glass Fibers

Composites are made up of reinforcement/filler components with a binder component when combined together; they have properties that are very different from the individual component's properties. The property of individual components combines together to give rise to the property of new materials [1]. The characteristics of composite materials are dependent upon the quality of reinforcement and matrix materials that form the composites. Glass fibers (GFs) are the preferred reinforcement materials when one of the required properties of composite is tensile strength or toughness. GFs are used mostly in the composite market, where it serves more than 95% of the raw materials in this field. Currently, the global consumption of GFs is more than 5 million metric tons, and among those fibers, E-glass fibers (E-GFs) are currently dominating the market [2, 3]. One of the reasons for this could be due to the fact that GFs, demonstrate comparatively high mechanical performance compared to the cost. In numerous composites, glass fibers occupy 70-75% of the weight and 50-60% of the volume of the structure [4]. Although in many of the cases, the application of GFs is in the composites where GFs are used in combinations with matrix, GFs can also be used without matrix [5]. For instance, fibrous blankets and filters used in

the area of thermal and acoustic protection are prepared from glass fibers without matrix. Moreover, GFs can also be used as an architectural membrane in the ceilings of airports and stadiums. GFs have been used heavily to reinforce plastics. As an example, in 2017, over a million metric tons of GF-reinforced plastics were produced. Furthermore, over 80% of the GF filament and spun GF are used for reinforcing plastics [6]. In upcoming years, due to the expanding economy, further increasing demand for high-strength constructions and building materials is going to boost already expanding glass fibers. The transparency and high-temperature withstanding capability of glass fibers have allowed them to be used as bio-composites in biomedical applications [7]. Today's glass fiber manufacturing follows a direct approach. In this approach, required raw materials are stored in silos, and afterward, following an accurate measurement, they are transferred into the mixing tank [8]. The fibers are usually available in different forms, such as roving, nonwoven mats, fibers, nonwoven mats, and even fabrics.

1.2 Glass Fiber Manufacturing Process

Production of GFs generally starts with melting naturally occurring materials such as silica clay, boric acid/colemanite, and limestone/calcite to produce the glass required for GFs. Modern glass furnaces are usually rectangular-shaped equipment, which has a narrow forehearth attached to one part, through which fiberizing process is done. The wall of the furnace is usually made of chromium oxides and baked with zircon and clay blocks. Natural gas is generally the choice of energy source in the furnaces. The schematic diagram in Figure 1.1 provides a generalized direct melt-spinning process of glass fiber production. Raw materials that are stored in the batch house are melted at a high temperature of around 1400-1700°C depending upon the composition of the glass. After leaving the furnace, molten raw materials pass through the channel where they are cooled and arrive at the forehearth. The molten raw materials are further preconditioned in the forehearth, and then molten glass enters the metal bushing, where the fiberizing process is done.

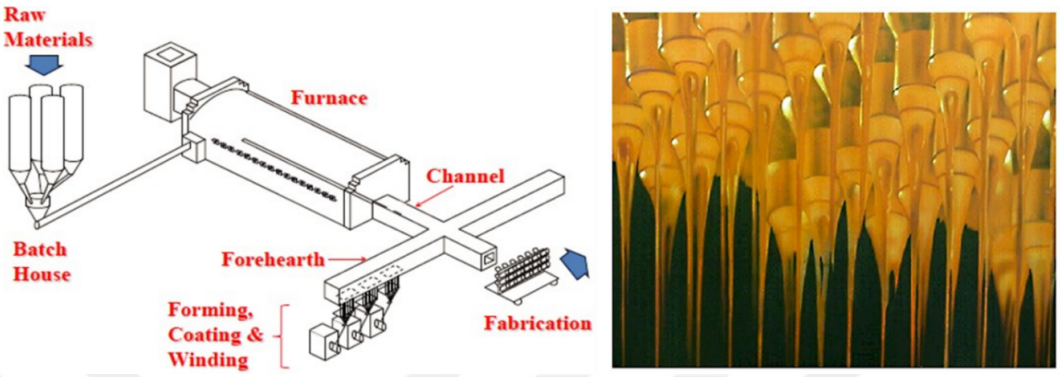

Figure 1.1: Schematic diagram of glass furnace with a magnified image of molten glass exiting from the bushing [4].

The bushing of GFs manufacturing spinneret is equivalent to the spinneret used in the synthetic fiber, except for the fact it is made of rhodium and platinum alloy or other alloys. Fiber flow through the nozzles having a diameter of 0.75 mm to 2.0 mm, and the pulling speed of the winder may rise to 60 m/s [9]. Fiber diameters can be altered by altering the speed of the winder [8, 9, 10, 11]. The fibers exiting from the bushing are cooled, and after applying sizing, materials are collected with winder on a bobbin (Figure 1.2).

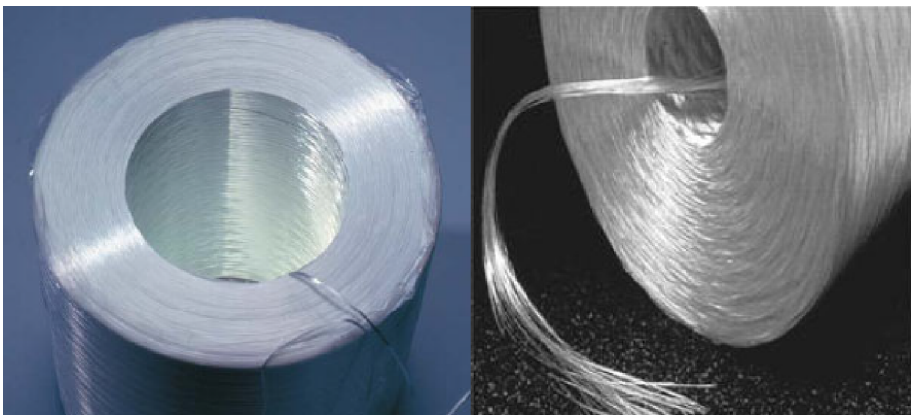

Figure 1.2: Stored glass fibers wounded in a Bobbin after exiting the bushing [4].

1.3 Glass Fiber Production Rate

Although the production and technology used in the GF industry have evolved over the years, the basic principles of production remained the same. Poiseuille's formulae can be used to describe the production rate (F) of E-glass fibers at the nozzle.

The rate of production (F) is related to the nozzle radius (r) with a length of (l), glass viscosity (η), and glass's height above the nozzle (h) by the following equation [8, 11]:

$$F \propto \frac{r^4 h}{l \times \eta} \tag{1.1}$$

From the equation (Equation 1.1), it can be understood that the fiber with a higher nozzle radius and lower viscosity is going to have a higher production rate.

1.4 Types of Glass Fibers

Glass fibers can be broadly classified into two categories; general application glass fibers, which are usually comparatively cheaper, and special application glass fibers, which are relatively expensive [7, 12]. Depending on the chemical compositions, the Glass fibers can be divided into different types such as S-glass, E-glass (with and without Boron), AR Glass, etc. [4, 8]. Among the glass fiber types, E glass fibers are the most widely used, as it produced for more than 90% of the application. The E glass fibers are also can be of two types; with boron and without boron. The percentage of silica (SiO_2) content differs between the two sub-classes of E-glass. E-glass without boron contains 59 to 61% SiO_2, whereas E-glass with 5 to 6% of boron contains 52 to 56% of SiO_2. However, this is also not a rigid rule, as the chemical content percentage not only differs from manufacturer to manufacturer, and it may even differ within the manufacturer depending on the availability of the raw materials in the geographical position

[6, 8, 11, 13, 14, 15]. In these categories of Glass fibers, S-glass is first produced by Owens Corning. This type of glass was developed to meet the demand of the ongoing composites industry. Its melting temperature is around 200 °C higher than the E glass fibers. Usually, E-glass fibers show an Elastic modulus of 80 to 81 GPa, whereas S glass Elastic modulus is around 86 to 87 GPa. AR glass fibers were first introduced by a British company named Pilkington brothers [6]. These types of glass fibers were developed for application in highly alkaline conditions such as concrete or cement reinforcement. This type of glass fiber contains a high amount of ZrO_2, and this proportion may range from around 15 to 23% . The melting point of zirconia is very high (2715 °C), and for this reason, Na_2O is usually added during the production process for lowering the melting temperature. This type of glass fiber exhibits an Elastic modulus of 72 to 74 GPa. This is the heaviest type of fiberglass available on the market [12]. E-CR glass is also known as chemical-resistant E-glass fibers. However, this is different than E glass. According to international standards, the E-CR glass contains up to 3% ZrO_2 and 3% TiO_2. ZrO_2 in E-glass fibers protects it from corrosion owing to the higher strength of the Zr-O bond compared with the Si-O bond [16]. Since this glass contains ZrO_2 and more than 1.5% TiO_2, it can not be considered E glass. Apart from these materials, E-CR glass may contain a maximum of 3% of Li_2O. This type of glass fiber exhibits a modulus of elasticity of around 80 to 83 GPa.

Table 1.1: Chemical composition of various types of glass fibers [6, 8, 11, 12, 13, 14].

Types	E-Glass (with Boron)	E-Glass (w/o Boron)	S-Glass	AR-Glass	E-CR Glass
SiO_2	52-56	59-60	60-65.5	58.3-68.6	58.2
B_2O_3	4-6	-	-	-	-
Al_2O_3	12-15	12-13	23-35	0.2	11.6
CaO	21-23	22-23	0-9	-	21.7
MgO	0.4-4	3-4	6-11	-	2
ZnO	-	-	-	-	2.9
TiO_2	-	-	-	0-2.8	2.5
ZrO_2	0.2-0.5	0.5-1.5	0-1	18.1-21.2	-
Na_2O	0-1	0.6-0.9	0-0.1	13.0-14.1	1
K_2O	0-0.2	0-0.2	-	0-2.8	0.2
Fe_2O_3	0.2-0.5	0.2	0-0.1	-	0.1
F	0.2-0.7	0.1	-	-	-

1.5 Glass Fiber Sizing and Coating

Glass fibers serve as the composite Industry's backbone, supplying more than 95% of the reinforcement materials to the composites industry [17, 18, 19]. Due to the delicacy of the fiber, sizing formulations is very critical for manufacturing glass fiber. However, due to the deep secrecy of not revealing the sizing formula in the industry, it is very difficult to have more than a superficial understanding of the blueprint of the size.

Size is essentially an organic-based coating material that is applied on the surface of man-made fibers during their manufacturing process to provide strength and guard them against fiber breakage. The process of applying size material on the surface of the fibers is known as sizing. In the literature, the words sizing and size are used interchangeably, which avoids the confusion that arises when people

may think "fiber size" means "fiber dimension." However, both terms "size and sizing" mean the same thing in this field.

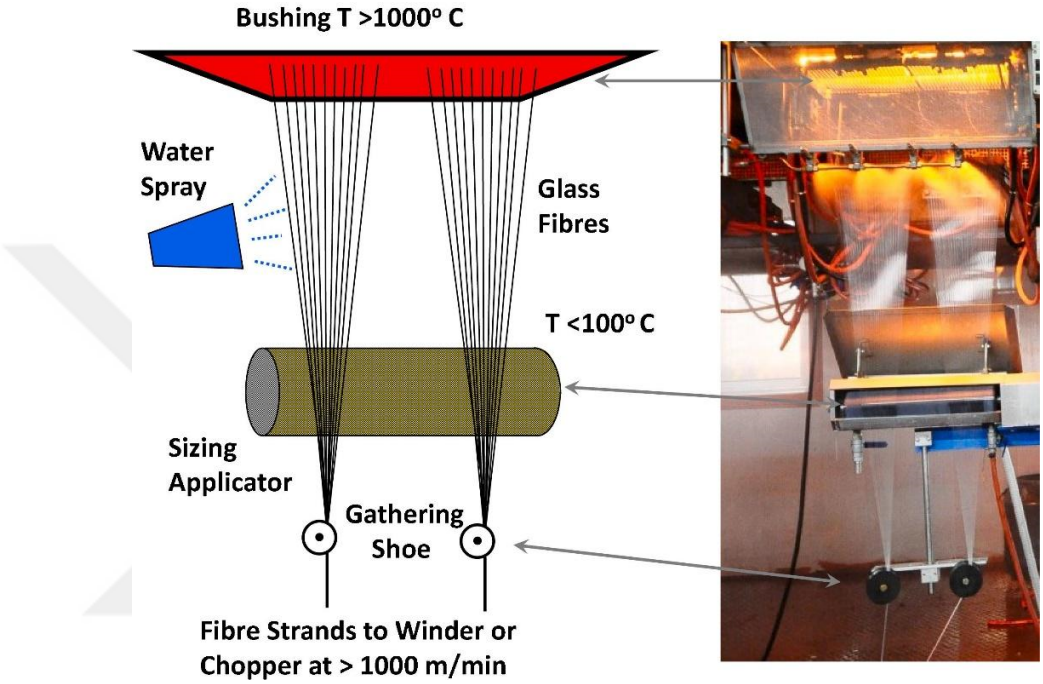

Figure 1.3: Schematic (on the left) and actual representations (on the right) of the fiber sizing process [20].

The above figure (Figure 1.3) shows a schematic diagram of the fiber sizing process. Size materials are usually applied via a sizing applicator. The sizing applicator consists of a size reservoir and roller, which is usually situated 1 to 2 meters below the platinum/rhodium alloy bushing plate. The fibers that are extracted from the metal bushing come in contact with the sizing in the size applicator. Size solutions/sizing are stored in the reservoir under constant circulation, and the roller rotates over the sizing applicator and attaches sizing materials to the fiber surface. The thickness of size of the fiber layer depends on the rotating speed of the roller. As stated earlier, complete knowledge of the complex formation of the sizing is difficult to obtain due to the secrecy of the materials [20]. In the literature, generic information about a coupling agent is given, where it is generally defined as water-based dispersion or emulsion having a complex formulation.

1.6 Glass Fiber Size Formulations

Glass fiber sizing contains a coupling agent, and in almost all cases for the coupling agent, organofunctional silane is used in glass fiber. The following general formula can define the coupling agent:

$$[Xi - Si(OR)_3]$$

here, R is a methyl/ethyl group, and X is a reactive group. Silane is a multifunctional component that not only links fiber and matrix but also provides hydrothermal resistance and improves the interphase of the composites. It is argued that non-coupling aspects of the coupling are more important for making a groundbreaking advancement in composites' performance. Silane works as a multifunctional component; it not only provides adhesion but also provides hydrothermal resistance and improves the interphase of the composites [20, 21]. In order to apply the silane-coupling agent to the surface of the fiber, it is first needed to be converted into silanol, and after that, when the water molecule is eliminated, it makes a covalent siloxane network with the fiber surface. When this fiber is used in other application, the X group of the siloxane network are capable of building a network with the other polymers or interphase. Over the years, many different components have been used as an X group. However, amino, methacryloxy, epoxide, and vinyl functional groups are the most preferred ones. Even among those, γ-aminopropyltriethoxysilane (APTES) is used more than the other types. In our study, we have made use of 1% APTES for chemically binding the nanoparticles with the fiber surface via the dip-coating method.

1.7 Function of Sizing in the Fiber Matrix Interphase

Glass fibers are very brittle materials hence prone to fracture, and for this reason, sizing materials are applied to the fiber after the spinning process. In general, the glass fiber sizing comprises a coupling agent (adhesion promoter), a film

former, a lubricant, and an emulsifier [22]. The sizing material not only provides protection for the fiber in the handling and production process but also can reduce the density of defects on the fiber surface [23]. The zone considering the fiber/matrix with the film former should be taken into special consideration to understand the effect of the film former. Hydrolysis and, following that, a polycondensation reaction of the silane-coupling agent with the aid of additives in this region resulted in a complex polysiloxane network (Figure 1.4).

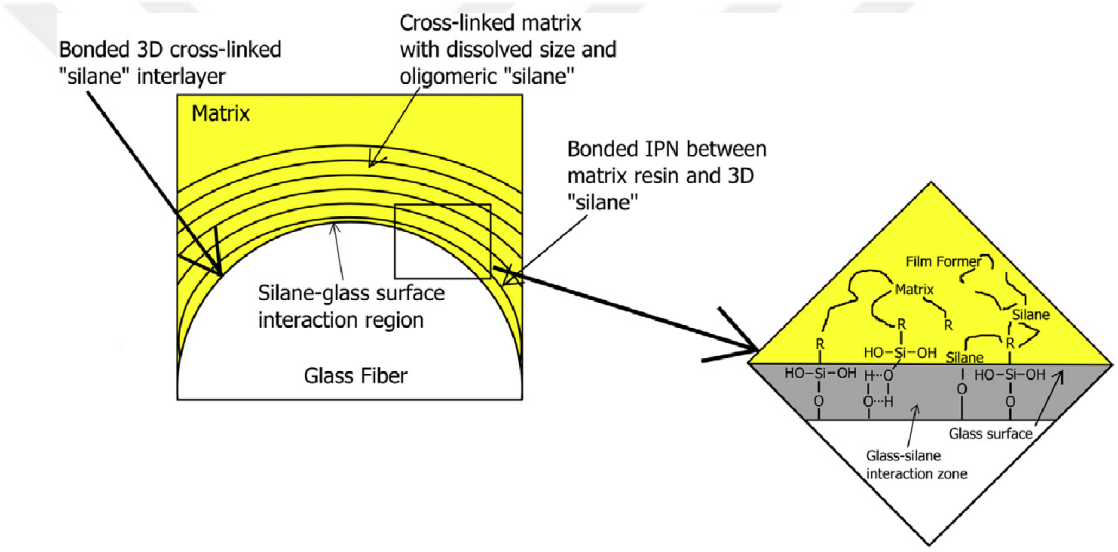

Figure 1.4: Schematic representation of the interaction of glass fiber with matrix and silane [22].

Moreover, in the polycondensation reaction process, hydrolyzed organosilane (silanol) may react with the hydroxyl group (OH-) on the surface of glass fiber to form a semi-interpenetrating network [24, 25]. The network results from the interactions of the cross-linked polysiloxane network with the linear polymer chain of film former [24].

1.8 Effect of Sizing and Nanoparticle on the Strength of Glass Fiber

Mechanical properties of the composite materials are dependent on the property of constituents of the composite material; fiber architecture, polymer matrix, and interphase region. In order to improve the performance of the interphase property of the composites, nanoparticles have been integrated into the fiber-matrix systems, which have impacted the composites' mechanical properties [26]. For instance, when the effect of sizing on the strength and energy absorption and strength capacities on E glass fibers were examined via the micro-debonding technique, it was discovered that organic resin and inorganic glass fibers compatible sizing is capable of increasing the adhesion and chemical bonding between glass fiber/epoxy resin system. Still, it decreased the energy absorption capacity and roughness of the surface [27]. Not only the type of sizing but also the sizing agent's distribution directs the mechanical properties of the carbon fiber composites and carbon fiber. It was found that small particle size and better distribution of sizing agent resulted in better wettability, higher (interfacial shear strength) IFSS, and aging resistance, improved interfacial bonding, and thus made a high-strength single fiber [28]. Interphase modification can also have a positive impact on the energy absorption and IFSS on the GF/epoxy composites. It was found that the addition of silica nanoparticles within the sizing is capable of modifying the fiber surface and thereby increasing the surface roughness of the fiber by more than three times. From the fractographic assessment, it was also revealed that the presence of silica nanoparticles encourages the crack to propagate in a tortuous path, consequently resulting in a higher energy dissipation [29]. Carbon-based nanomaterials such as carbon nanotubes (CNTs) are also found to be useful in improving the shear strength of the GF/epoxy (EP) and carbon fiber (CF)/EP composites [30, 31]. Electrophoretic deposition of CNTs on CF fabric for CF/EP composites improved the composites' fracture toughness and shear strength. The fractographic inspection also revealed the presence of CNTs on the interlaminar region and strong adhesion between the carbon fiber (CF) and CNTs, which may have contributed in the enhanced mechanical properties [31].

Incorporating nanomaterials into the sizing materials have multiple benefits. Firstly, nanomaterials integrations led to an increase in the fibers' surface roughness. Secondly, it increases the interphase's local modulus, thus positively influencing the shear strength. Finally, it also allows taking advantage of the structural property possessed by the nanomaterials and sensing application [22, 32]. Moreover, surface roughening has far-reaching benefits. When a crack is developed at the interphase or rough surface of the fiber, and if the surface of the fiber is rough, it forces the propagation of the crack into a zigzag route instead of a planar one, which allows the materials to absorb more energy. As the crack propagates in a zigzag route, it gives more time to dissipate energy, causing the toughening of the materials. Nanomaterials integration can also have applications in structural health monitoring; it was reported that by using CNTs as nanomaterials, it is possible to detect strain, stress, and damage in the composites [32]. Analyzing the progress in this field from the published literature over the past few years, the authors have found that research in that area has moved into developing smart interphase. For instance, E-GF/PP micro-composites prepared by solution coating of 0.5 wt.% of Single Wall Carbon Nanotube (SWCNT) added sizing solution have found its usefulness as strain sensors. Moreover, nanofiller materials have also positively improved adhesion, and it could also monitor interphase property variations [33]. Multiwall Carbon Nanotube (MWCNT) was also found to play a role in this area of smart composites—the addition of 0.5 wt.% MWCNT dispersion to EP-compatible phenoxy sizing enhanced the glass transition temperature (Tg) and marginal improvement of crack initiation energy (Gic). Also, the effect was found to be more prominent in the bulk matrix as opposed to sizing [34].

1.9 Mechanical Properties of Glass Fibers and Reason for Discrepancy with Theoretical Value

Over the last few decades, glass fiber and glass fiber reinforced composites have been experiencing steady growth in the industry of automotive, wind turbine blades, printed circuit boards, and consumer goods [35]. Although there are different types of glass fiber, E-glass is principally employed, and it is mainly composed of CaO, SiO_2, and Al_2O_3 and 0-10 % of B_2O_3. It has also found its use in PCB (Printed Circuit Board) electronics and industrial applications because of its superior mechanical, chemical, and electrical properties [13, 35, 36]. There are notable differences in the measured and theoretical value of the Young modulus of the glass fibers [37], which indicates that there is a gap between theory and practice. The differences in theoretical value and practical values are caused by myriad reasons. Firstly, alkali (Na_2O, K_2O, Li_2O), alkaline earth (CaO, MgO), and their relative proportions have varying effects on the local and surrounding oxygen structure of the glass network former (SiO_2 and B_2O_3) and local network formers (Al_2O_3). Their concentrations may increase the bonding of the glass network, which results in a higher Young modulus, and when it decreases the bonding of the glass network, it results in a lower Young modulus [38, 39, 40, 41, 42]. Secondly, the thermal history of glass affects the molar volume, fictive temperature, and density of the glass fiber. For this reason, the annealing of glass results in a high Young modulus as the annealing results in a low fictive temperature and high density for the annealed glass compared to the quenched Glass [43, 44, 45].

Surface flaws have one most negative impact on the strength of the glass fibers. The surface flaw is the reason why the fibers fail below the theoretical value of the tensile strength. If there is any flaw in the surface of the glass fiber, it allows the stress to concentrate on the flaw and thus ultimately causes the failure of the fiber. These flaws are usually introduced when the fibers are exposed to a corrosive medium such as acid, basic, and water vapor, or they can also be introduced

during handling and the use of materials [46, 47, 48, 49]. Practically, it is nearly impossible to keep fibers away from any contact, and hence, the flaws are usually introduced before the material is even subjected to a test. Additionally, glass fiber strength is actually an extrinsic property and is the result of a combination of thermal history, testing temperature, chemical composition, and atmospheric conditions [35, 50, 51].

1.10 Characteristic Properties of Glass Fibers

The composite's characteristics are heavily affected by the property of reinforcement glass fibers, and the characteristics of the glass fibers are dependent upon the fiber diameter, text, fiber pulling speed, and several other factors [4].

Fiber diameter: It is dependent upon the pulling rate of the bushing. In general, finer fibers have a higher tensile strength because the low volume of the fine fibers allows them to come in less contact with the flaw-inducing obstruction. For the fabrication of composites, rovings generally pass through different guidelines, and if the rovings are in fine sizes, they can easily pass through the bent guidelines, which also preserves their property and contribute to the increased tensile strength of materials [13].

Tex: Tex is the most widely used metric to measure the weight of glass strands worldwide. It is basically the linear density of fiber in g/km. The Tex of a fiber is dependent upon the design of the bushing and the expected diameter of the fiber. If the bushing diameter is the same, the fiber with a small diameter will have a lower tex compared to the fiber with a higher diameter. The tex of glass fiber strands ranges from 300-4800. Practically, the tex of a fiber can be increased or reduced by changing the speed of the winder of glass fibers. High-tex fibers usually provide more coverage on the composite laminate compared as opposed to fiber with low-tex. Consistency of tex is critical in the composites' performance, especially in high-performance applications such as aerospace, defense, and security equipment [4].

Other Factors: Apart from these materials, sizing is also important in determining the quality of the glass fiber performance. The oxidation state of iron in melt solution has a significant effect on the mechanical properties of glass fibers. Iron (Fe), which acts as a network modifier in glass, controls the viscosity, fiber-cooling rate, and fiber tension and thereby owns the property of the finally produced glass fiber [52, 53, 54, 55]. This stability of the iron is generally adjusted by careful selection of reducing and oxidizing agents.

1.11 Flaws in Glass Fiber

The strength of glass fibers is a very critical factor, and for this reason, it has found its usage in aerospace, structural reinforcement, automobile, and even in military applications. The chemical composition, thermal history, forming condition, used sizing, and composite design characteristics all affect the practical strength of the glass fiber. However, the experimental strength is much lower than the theoretical strength, which indicates that a minor defect present on the fiber surface or within the fiber have far-reaching consequence; it acts as a concentrator of stress, causing a decrease in the overall strength of the glass fiber. It is possible to minimize the defects by optimizing the glass forming and melting techniques, but producing defects-free glass is nearly impossible [15]. This section describes two of the most accepted theorems (Griffith's theory and Orowan's Theory) about glass fiber's flaws in detail.

1.11.1 Griffith's Flaw Theory

Although studies on the fracture of glass have been in the literature since the early 19th Century, people were unaware of why a glass fiber breaks at a particular strength until the work of Griffith in 1920 [14, 56, 57]. Griffith has found two important formulae for explaining the behavior of glass fibers at that time. In the first one, he noticed the strength of the glass fiber has a relationship with the size of the specimen. From this observation, he concluded that glass fibers surface

contains flaws in the surface. For this reason, if the larger sample is exposed to the specimen, the probability of having a flow is more, and hence it results in a lowering of strength.

Inglis first made the assumption that applied force on the glass acts as a stress concentrator to the area where defects are present, and this could be either in bulk or on the surface. However, this was hypothesized by Griffith, who formularized that not all the flaw in the glass causes the failure of glass. A flaw in the glass has to be a certain critical length before it starts to propagate on the fiber. Apart from that, failure will occur in the place where the most severe flaw is located. According to Griffith, a glass with Young's Modulus (E), interfacial surface energy (γ), and critical depth length of crack (c*) can withstand a maximum failure stress (σ_f) by the following formula;

$$\sigma_f = \sqrt{\frac{2E\gamma}{\pi \times c*}} \tag{1.2}$$

This is also analyzed in detail by the following authors [14, 15, 56]. This equation explains that the actual strength of the glass fiber is contingent upon Young's Modulus (E) and interfacial surface energy (γ), which is dependent on the composition, thus indicating the final strength of the glass fiber has a direct dependence on the chemical composition of the materials.

From the literature, it is also well known that if there is the presence of any water molecules or bubbles at the surface of glass fibers, it leads to a decrease in the interfacial surface energy required to fracture the material [58, 59].

1.11.2 Orwan's Theoretical Strength

In Glass terminology, Orowan defined the maximum stress (σ_m) is the stress required to separate two atoms of the glass fiber at a distance of (a) and with a surface energy of the pristine fiber (γ) by the following equations;

$$\sigma_m = \sqrt{\frac{E\gamma}{a}} \tag{1.3}$$

When, E = 70 GPa, a = 0.2 nm, and fiber surface area gamma = 3.5 J/m^2 were used for typical silicate glasses, the computed theoretical stress was found to be 35 GPa. However, in practical circumstance, the strength range between 400 to 500 MPa, which has a very high discrepancy with the theoretical strength. For this reason, it is stated that the real strength of the glass fiber is much lower than the theoretical strength owing to the presence of structural flaws. According to Orowan, interatomic strength depends on the glass fiber's surface energy, elastic modulus, and structure. Moreover, when the glass fibers undergo fractures, it creates two new surfaces, and previous chemical bonds between the atoms are broken. However, when the fracture strength is measured, there is a significant difference between the theoretical and practical strength observed in practice [56].

According to Orowan, interatomic strength depends on the glass fiber's surface energy, elastic modulus, and structure. Moreover, when the glass fibers undergo fractures, it creates two new surfaces, and previous chemical bonds between the atoms are broken. However, when the fracture strength is measured, there is a significant difference between the theoretical and practical strength observed in practice [56].

1.12 Fractography

Fractography can be defined as the field of engineering where a fractured surface is studied to obtain information about the failure of materials. It is not very difficult to observe the fracture origin in the float glass, and even possible to estimate a relationship between the fracture surface and the strength.

When someone investigates the fracture surface, a typical fracture pattern can be seen in Figure 1.5. When a fractured surface is observed under the microscope, a characteristic pattern can be seen around the initial flaw. The first region is

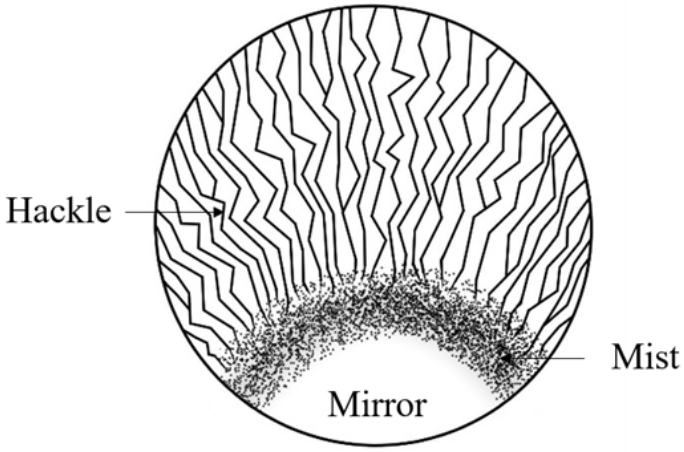

Figure 1.5: Schematic representation of the cross-section of glass fiber fractured by tensile force, indicating mirror, mist, and hackle region [56].

very smooth and known as the mirror region. The next region where a very small band with a slightly rough area is observed is known as the mist region. Finally, the roughest region of the fractured surface is created, also termed the hackle region (Figure 1.6).

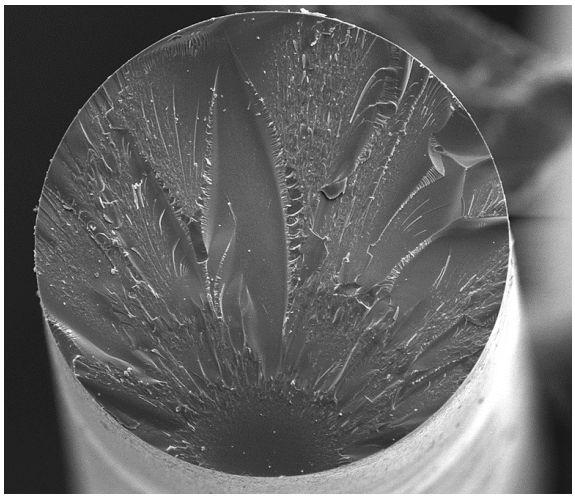

Figure 1.6: SEM image of the cross-section of glass fiber fractured by tensile force [19].

From the literature, it is found that the strength of fiber depends on the size of the mirror-mist zone and mirror-hackle zone. According to the literature, failure stress (σ_f), is related to the mirror-mist region (r_m) and mirror-hackle region (r_h)

by the following formula,

$$\sigma_f = \frac{A_m}{\sqrt{r_m}} = \frac{A_h}{\sqrt{r_h}} \tag{1.4}$$

where, A_m and A_h are the constants whose values are (1.7-1.9) and (2.0-2.1), respectively [60, 61, 62].

1.13 Tensile Strength Analysis by Weibull Statistics

Glass fiber is very brittle in nature, and for this reason, it has a wider distribution of tensile strength. Moreover, the fiber's tensile strength depends on the surface flaws, which are malleable to statistical analysis [63]. According to the "weakest link" theory, a material breaks down at a point when the felt stress on any point exceeds the capacity of surrounding materials to withstand the local stress. Weibull Distribution is widely employed for analyzing the tensile strength of brittle materials like glass and ceramic owing to the mathematical simplicity and excellent compatibility in its application. It is a cumulative distribution function, which is based on the "weakest link hypotheses." This hypothesis state that the weakest link in the materials initiates the fracture, and it cannot be initiated by the smaller flaws [56, 64]. Apart from this assumption, a few more physical assumptions are made for this distribution;

- The strength of the materials is independent of time.
- The compressive strength of the materials has no contribution to the fracture.
- Individual flaws have no interactions with each other.
- Material fracture is governed by a single-flaw population.

A material with a probability of fracture (P), fracture strength (σ_f), threshold strength (σ_u), scale parameter (σ_0), and the Weibull Modulus (m) can be mathematically defined by the following equation;

$$P = 1 - \exp\left[- \left(\frac{\sigma_f - \sigma_u}{\sigma_0} \right)^m \right] \tag{1.5}$$

here, threshold strength (σ_u) means the strength below which a fracture cannot be initiated, and the scale parameter (σ_0), is a characteristic strength that corresponds to a fracture probability of 63.2%. Weibull modulus and the scale parameter cannot be negative values, and the former one shows the scatter of the data. It can be estimated that if a material has a large value of m, the probability of the flaw is lower, and the material is expected to have a higher strength.

The distribution written in the above equation is called the 3-parametrical Weibull Distribution. This distribution is very complex as it is very difficult to measure the required data from the given equation. Consequently, a 2-parametrical Weibull distribution is used, considering. (σ_u=0), since the fibers having a strength value of almost zero will be broken before the start of the test. Substituting (σ_u=0), in the 3-parametrical Weibull distribution, the equation converts into,

$$P = 1 - \exp\left[- \left(\frac{\sigma_f}{\sigma_0} \right)^m \right] \tag{1.6}$$

This function is also dependent on the assumption that the fracture has occurred due to one type of flaw [64]. However, if there is more than one type of flaw present 3-parametrical Weibull distribution function can be used, and on this occasion, the plotted graph will not result in a straight line [64].

Now, if you take the double logarithm of the above equation and rearrange it to the other side of the equation, it converts the exponential function into the following equation,

$$ln(ln(\frac{1}{1-p})) = mln(\sigma) - mln(\sigma_0) \tag{1.7}$$

This equation can now be compared to the simplest linear algebra equation Y=Mx+b, whereas,

$$Y = ln\left(ln\left(\frac{1}{1-P}\right)\right)$$
$$X = ln(\sigma_f)$$
$$b = -mln(\sigma_0)$$

The slope of equation (1.7) will give the Weibull modulus or the scatter of the tensile strength, and the scaling parameter (σ_0), can be calculated from the intercepts of the graph. Different authors have used different methods for calculating the cumulative probability of the failure (P_i), and determining the cumulative probability of failure of the i_{th} term can be calculated with the least biased values [64] from the following equations for the (N) value of up to 50 [65].

$$P_i = (\frac{i-0.5}{N}) \tag{1.8}$$

1.14 Effect of Sizing and Nanoparticle on the Strength Of Glass Fiber

Not always, the incorporations of nanofillers into composites matrix system have a desirable positive outcome. For instance, analysis of the effect of 20% silica nanoparticles on CF/EP composites has found that silica nanoparticles do not positively impact interfacial bonding [28]. On the contrary, modification of the matrix by 1D CNT, 2D nanofillers have been found to improve the ILSS by up to 15% when only 0.3% functionalized CNTs were added to this solution [66]. According to another paper, incorporating graphite nanoplatelets (GNP) and clay to bulk EP actually increases the IFSS to GF. Improved IFSS of about 30%

was attributed to the enhanced GF/EP wettability, GNP's favorable effect on the chemical interaction between GF/EP, and EP matrix's improved mechanical property [67, 68]. Previous research has been done in this field to understand the impact of different types of nanomaterials/2D materials on the mechanical characteristics of GF or GF/EP composites, and mixed results were found in the literature. For instance, when the mechanical property of Glass fiber (GF)/Epoxy (EP) composite prepared with the aid of a hybrid sizing agent was investigated, it was discovered that the IFSS and wetting ability of the composite have been positively affected by the hybrid-sizing agent. However, there was no major impact on the tensile strength of the composites [69, 70]. Not only the nanoparticle types but also the methods of integrating nanoparticles can have different impacts on the mechanical properties. When CNT was deposited on E-glass fiber by the electrophoretic deposition (EPD) technique, it led to an increase in the IFSS strength of the single glass fiber, as it changed the modes of fracture in the CNT-coated fibers. However, it was also noted that this method has a minor impact on the tensile properties of E-glass fiber [26]. On the contrary, when CNT was grafted on glass fibers by the dip-coating method via the assistant of Nafion, it improved the tensile strength by 38% and IFSS by 116% . However, it did not alter the elastic modulus of the fiber [71]. During the formulation of composites, nanoparticles can be grafted on fiber sizing, matrix, or both fiber sizing and the matrix. When this was investigated for CNT, it was found that IFSS has been increased for all the combinations, but it has the most increase when the CNT was integrated into the sizing of the fiber [72]. It is not always true that the incorporation of nanoparticles has always had a positive effect on the mechanical property of glass fibers. When 2% graphene was incorporated into the glass fabrics via a blade coating approach for preparing composites, it decreased the flexural strength, flexural modulus, and tensile strength by 26% , 37% , and 39% , respectively [73]. Nanoparticle integration has been successful in improving the mechanical properties of organic fibers such as flax-fiber/EP composites. According to earlier studies, coating and grafting with nanoparticles such as ZrO_2, TiO_2, and CNT have the capability to repair surface flaws, which in turn enhances the mechanical property of the glass fibers. Moreover, It was also reported that grafted nanoparticles such as Titania (TiO_2) [74, 75, 76, 77]

and zirconia (ZrO_2) into the fiber, matrix, or both the fiber and the matrix could act as a bridge for transferring the loads, and are capable of delaying crack propagation and subsequently improving the tensile strength, flexural strength, shear strength, interfacial shear strength, the storage modulus of the composites [78].

1.15 Objective

From the above discussion, it is understood that the mechanical property of glass fiber greatly depends on the surface defects, structural impurity, size and shape of the fiber, atmospheric condition, thermal history, and raw materials composition [35, 50, 55, 19, 79]. Improving the mechanical and chemical properties of glass fibers are necessary to meet the ever-increasing demand for higher strength in the fiber-reinforced composites industry. Surface impurity and imperfection are the reason glass fibers exhibits a significant difference in theoretical and experimental strength values.

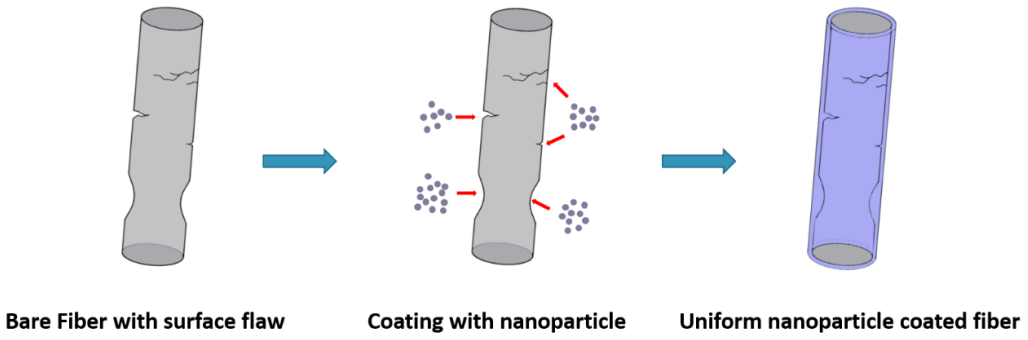

Figure 1.7: Schematic representations of the glass fiber healing process by nanoparticle coating.

The aim of this thesis is to anneal the surface flaw present on the E-glass fibers by the integration of nanoparticles in an industry-friendly, cost-effective way to produce uniform homogeneous glass fibers. For this purpose, E-glass fibers were dip-coated with titania (TiO_2), silica (SiO_2), and zirconia (ZrO_2) nanoparticles to reduce the effects of surface defects and protect them from further damage. The mechanical property of nanoparticle-coated single E-glass fibers

is investigated using Weibull's statistical analysis. Additionally, the chemical stability of the nanoparticle-coated fibers is investigated under highly alkaline solutions. A fractographic examination was further carried out to observe the effect of coating on the fractured surface's mirror region.

Chapter 2

Experimental Methodology and Procedure

2.1 Methodology

For analyzing the chemical and mechanical properties of E-glass fibers, a range of spectroscopic, mechanical, and chemical characterization techniques were utilized in this study. Raw materials for the study, E-glass fibers, and silane coupling agent (APTES) were supplied by the project partner SISECAM Inc., and nanoparticles were purchased from Nanografi, Turkiye. E-glass fibers were modified using nanoparticles, coupling agent, and heat treatment, and after that, different spectroscopic, mechanical, and chemical analysis techniques were carried out via Scanning Electron Microscopy (NanoSEM), Environmental Scanning Electron Microscopy (ESEM), Atomic Force Microscopy, Micromechanical Analyzer, and X-ray Photoelectron Spectroscopy (XPS). This chapter provides a detailed description of the processes from sample preparation to analyses that were utilized in this study.

2.2 Sample Preparation for Tensile Test

Preparation of the sample for this study is a multi-step process. It can be divided into six steps; chopping of fibers, preparation of nanoparticles solution, preparation of APTES solution, preparation of cardboard sample holder, dip coating of nanoparticle-coated fiber, and fixation of the fiber on the window-shaped sample holder.

E-glass fibers used in this study supplied by our project partners SISECAM Inc. were chopped into a fine length of about 40 to 50 mm in size. These fibers have an average diameter of around 60 to 75 μm. In the following steps, pure nanoparticles of mass concentration (w/v) % solution (Nanografi, Turkiye) are diluted using deionized water (DI) water to prepare nanoparticles solution of the required concentrations. Mass concentrations (w/v) % solutions were prepared for nanoparticle solutions, and for preparing the APTES solution, volume percentage (v/v) % were considered. Although the concentration of nanoparticles varied for different experiments, the concentration of the APTES remained at 1 (v/v) % in all the experiments. In order to compare the effect of nanoparticles on the mechanical and chemical properties of E-glass fibers, bare fibers were also prepared by the same process. The only difference was that in the first dip-coating process, they were only dip-coated with DI water to have a reliable comparison with nanoparticle-coated fibers. The rest of the process was the same for both the bare and nanoparticle-coated fibers.

The figure below (Figure 2.1) shows a schematic diagram of the fiber dip-coating process. In the beginning, chopped fibers are dip-coated using the required concentration of nanoparticles in a petri dish. In the next step, the nanoparticle-coated fibers are annealed in the furnace at 120 °C for 30 min under the vacuum to evaporate the excess water and allow optimum chemical binding conditions. After that, the nanoparticle-coated fibers are coated with a 1% (APTES) agent to allow chemical bonding of the nanoparticles to the fiber surface. The APTES is a multifunctional component that promotes adhesion, provides hydrothermal resistance, and forms a polysiloxane network. Besides,

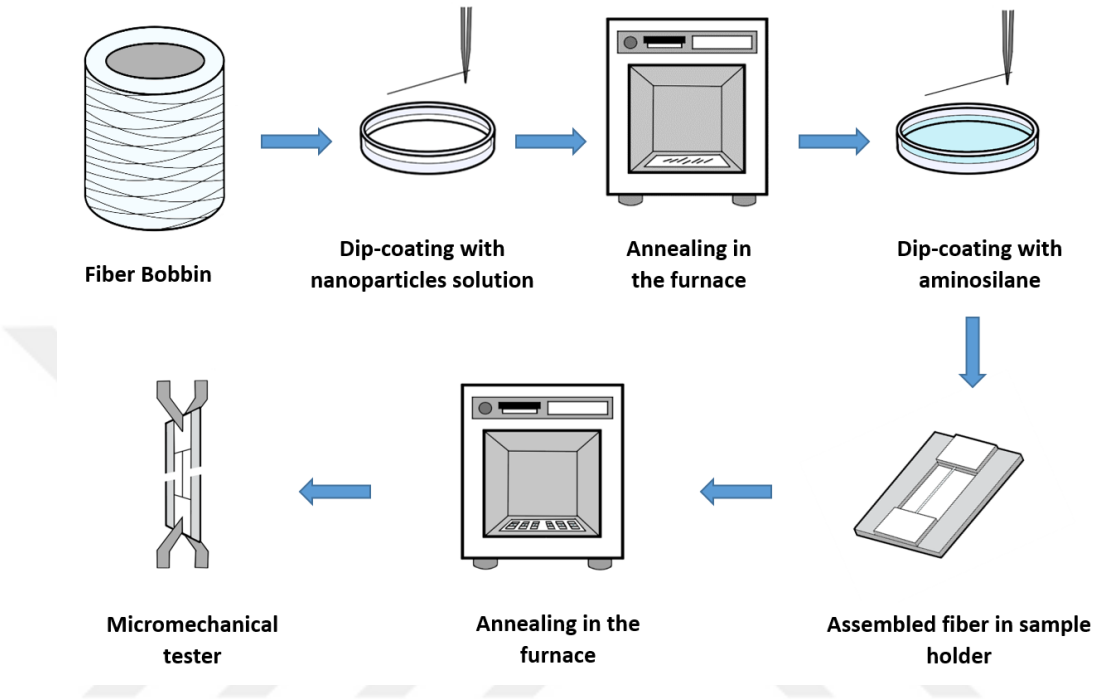

Figure 2.1: Schematic diagram illustrating the sample preparation process for the tensile test [19].

it is also possible to attach nanoparticles on the fiber surface without APTES [80]. However, we have dipped the fibers in APTES to improve the adhesion of nanoparticles onto the surface of glass fibers and promote hydrothermal resistance [20]. Following that, the nanoparticle-silane-coated fibers were mounted on a window-shaped cardboard holder and attached with a commercial adhesive. In the next process, the fibers are put inside on furnace at 120 °C for another 30 minutes under the vacuum to evaporate excess water and allow time for further chemical bonding of silane with nanoparticles. After that, the prepared samples are taken to the micromechanical analyzer for the tensile test.

2.3 Mechanical Analyses of the Tested Fibers

In order to know the tensile strength and probability of the failure of the E-glass fibers, it was analyzed under a micromechanical analyzer. Glass fibers' tensile

strength was calculated using a Micromechanical analyzer (Instron 5960) with a cross-head speed of 1 mm/min based on ASTM D3832M-14 [26]. The average diameter was considered for determining the fiber's tensile strength and for speeding up the process. However, after the experiment, the accurate measurement of the diameter of the fibers was calculated using optical microscopy (ZEISS AX10), and this allowed us to calculate the actual value of the tensile strength for the individual fiber. As mentioned, the fibers are mounted on window shaped sample holder. The cardboard holder is rectangular with a dimension of 45 mm to 35 mm in size, whereas it has a window of 35 mm to 25 mm at the center (Figure 2.1). One frame of the window is cut before gripping the sample on the micromechanical analyzer, and the second window is cut after gripping the sample holder on the micromechanical analyzer. This allowed the tensile force only to be applied on the fiber. The fibers are pulled vertically via the grip of a micromechanical analyzer. When the window-shaped cardboard holder is pulled through the tensile tester, it applies force to the cross-sectional area of the fiber, and as a result of the applied stress, the fiber experiences fracture. This stress is mathematically defined as the tensile strength of the fiber. Around 50-60 fibers were used to test this fiber, and almost 50-60% of the fibers broke within the window, meaning that it is broken purely by tensile strength. The fibers which broke at the edge or inside the grip of the sample holder and the fibers which slipped from the cardboard were eliminated from the study. The fibers, which were broken in other regions, i.e., edge, were omitted from this study to ascertain there was no mistake in the calculation. Additionally, testing around 30 samples provides a 96% confidence level of the data.

So mathematically, we can define stress (σ) by,

$$\sigma = \frac{F}{a} \tag{2.1}$$

where, A=$(\pi d^4)/4$, (σ) is the tensile strength of the fiber, (F) is the applied force, which is applied via the grip of the micromechanical analyzer, and (d) is the diameter of the fiber. After the tensile strength, Weibull analysis is also done to determine the probability of the failure of the fiber under a given strength.

2.4 Sample Preparation for Alkaline Test

The schematic diagram (Figure 2.2) illustrates the procedure for doing the fibers' alkaline-resistant test. Only ZrO_2 nanoparticle-coated fibers were considered for the alkaline test. Firstly, BFs are dip-coated using nanoparticle solutions of 5%, 10%, and 15% ZrO_2 solutions. After that, the fibers were annealed in the furnace for 30 minutes at 120°C. In the next process, the nanoparticle-coated fibers are coated again with 1 amino silane and put onto the furnace for another 30 min at 120°C. Following that process, the fibers are mounted on the cap of the chemical containers. After that, the fibers were submerged in the 0.316 M alkaline solutions, which made a pH of 13.5 for 4 days. Bare fibers, 5%, 10%, and 15% ZrO_2 nanoparticle-coated fibers were used. After that, topographic, elemental, and compositional analysis of the surface was carried out using SEM.

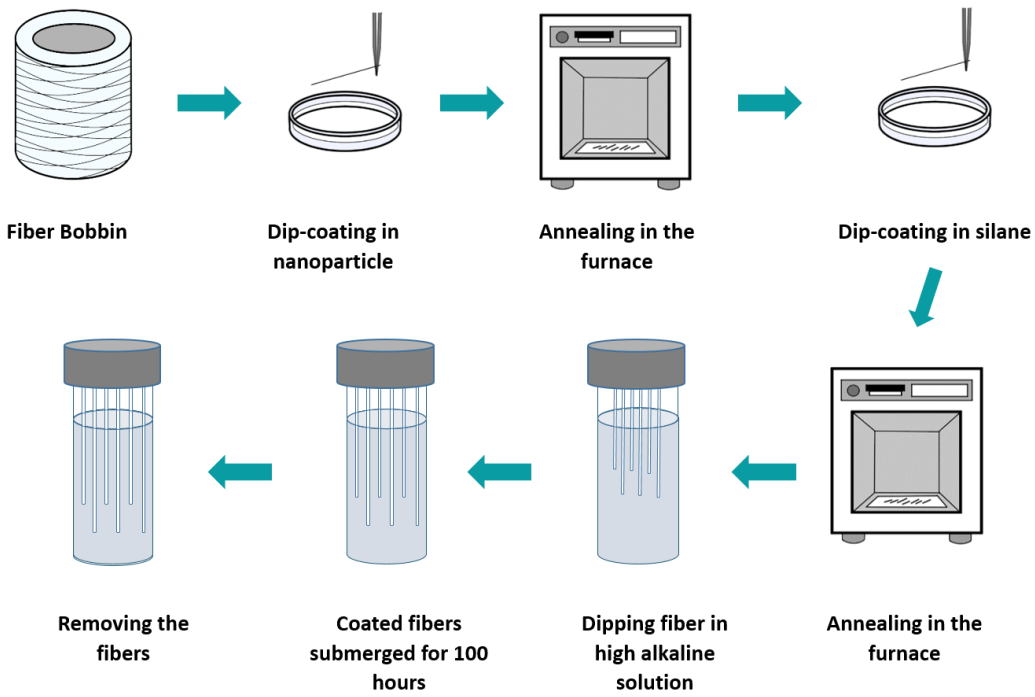

Figure 2.2: Schematic diagram of experimental procedures for the alkaline resistance study.

2.5 Characterization Techniques

Different characterization techniques are used in this study to know the surface morphology and to analyze the fracture behavior of nanoparticle-coated fibers. In order to see the surface of nanoparticle-coated fibers, the dip-coated fibers were investigated under the Scanning electron microscope (SEM; Nova NanoSEM 430), Atomic force microscopy (AFM; Veeco Dimension 3100), X-ray diffraction (XRD; Pananalytical X'pert Pro, Cu K-alpha) and X-ray photoelectron spectroscopy (XPS; Thermo Scientific K-alpha). The SEM showed the presence of nanoparticles on the surface of glass fibers and the effect of corrosion on the fiber surface. AFM also provided additional evidence of the existence of nanoparticles on the surface of the nanoparticle. Furthermore, XRD revealed information about the crystal structure of the nanomaterial, XPS provided information about the bonding of nanomaterial with the fiber surface, and EDX analysis revealed elemental and compositional information about the materials.

2.5.1 Scanning Electron Microscopy Analysis

Scanning Electron Microscopy (SEM) is a widely used instrument for investigating materials features even below the micro level. In this microscopy, the electrons are produced by an electron gun, which is then directed on the sample via different lenses. The incident electron beam is directed at a specific location of the sample, which ejects secondary electrons, backscattered electrons, and X-rays. Different emission contains different information about the sample. For instance, secondary electrons provide topographic information, backscattered electrons provide information about composition, and X-ray contains information about elemental composition. These emitted electrons and X-rays are collected via a detector, which converts them to a signal, and produces the final image on the screen of the monitor. In order to generate all of these emissions, the sample surface has to be conductive. Since E-glass fibers were non-conductive, it was coated with an Au/Pd layer of 10 nm via Precision Etching Coating System (PECS).

2.5.2 Atomic Force Microscopy

Atomic Force Microscopy, shortly known as AFM, is a specific type of scanning probe microscopy (SPM), which has a proven resolution on the order of nanometers. AFM provides three dimensional (3D) image of a sample via the measurement of force acting between the AFM tip and surface. The tip of AFM is supported by a flexible cantilever which is generally made of silicon nitride or silicon [81]. In AFM, on the top of the cantilever, there is a tip, and the tip measures the forces acting between the surface and the tip on the principle of Hooke's law. The deflection of the cantilever produces numerous data about the surface of the sample. Based on the types of samples, AFM has three modes of working, such as contact mode, intermittent contact mode (tapping), and non-contact mode [82]. In our work, we utilized the AFM (Veeco, Dimension 3100) of our project partner SISECAM for investigating the morphological analysis of our nanoparticle-coated sample.

2.5.3 X-ray Photoelectron Spectroscopy

X-ray photoelectron spectroscopy (XPS) is a powerful material characterization technique that is used for the surface analysis of materials. This useful technique is based on the photoelectric effect. When the incident energy of a photon reaches a sufficient level of energy, it moves the electron from the initial state to the excites state. This excited electron is then emitted as a photoelectron. The energy of emitted photoelectrons depends on the chemical composition of and surrounding chemical atmosphere. The number of electrons is related to the concentration of the emitting atoms in the sample. Every element has a different electron binding energy. As a result, it makes it possible to identify different elements from their binding energy. Moreover, the binding energy of the electron is also dependent upon the surrounding electronic environment. When an electron reacts with another electron that has different electronegativity, it also leads to a change in the binding energy. Analyzing these binding energy reveals details about a molecule's chemical information. XPS is capable of producing information about

the top 10 nm of the surface except for the elements hydrogen (H) and helium (He).

2.5.4 X-ray Diffraction

The X-ray diffraction method is the widely used technique for measuring the crystallinity of materials. In this method, X-rays of high energy and very small wavelength are bombarded on the material. When this X-ray passes through the materials, this ray interacts with the atoms. As a result of interaction, constructive and destructive interference of the scattered wavelength can occur. Due to this interaction, it results in higher and lower intensity emissions. When the X-ray interacts with a plane of a material, it results in a peak of higher intensities, and a sharp peak can be seen on the detector of the XRD. On the other hand, when the X-ray interacts with the amorphous material, due to the absence of any crystalline structure on the materials, the rays are emitted in all directions, and this results in very broad range peaks on the XRD spectrum. The detector of the XRD detects the intensity as well as the diffraction angle of the materials. By analyzing these results with Bragg's law, the atomic arrangement of the materials can be revealed.

Chapter 3

Titania Nanoparticle-coated Fibers

3.1 Introduction

The mechanical properties of glass fiber composite depend on the reinforcement materials, matrix, and sizing materials. Due to superior mechanical performance, low weight, and affordability, Glass fibers have been frequently employed as reinforcement or filler materials [20, 83]. Enhancing the quality of reinforcement materials can contribute to the improved property of the composites. Surface defects, structural impurities, raw materials, and thermal history can contribute to the final property of the composites. From the other work, it was found that metal oxide nanoparticles such as titania (TiO_2) and zirconia (ZrO_2) work as a bridge between fiber and matrix, consequently enhancing fiber matrix interaction and causing an improvement in mechanical characteristics of the composites [73, 76, 77]. These oxides form a major proportion of GF. GF-compatible metal oxides such as TiO_2 can be a very good candidate for studying the effect of GF's mechanical and chemical properties. In this chapter, In order to improve and produce a uniform glass fiber, E-glass fibers are dip-coated with rutile TiO_2 nanoparticles (average dia 47 nm) for healing the surface flaw and impurity present on

the fiber surface. Microscopic and spectroscopic analysis proved the presence of TiO_2 nanoparticles on the surface of E-glass fibers. Weibull distribution was also employed to know the effect of nanoparticle coating on the mechanical properties of glass fibers. Besides, the fractographic study was conducted on bare fibers and TiO_2 nanoparticle-coated fibers to see the fracture behavior of the nanoparticle-coated fibers.

Table 3.1: Naming conventions used for studying the effect of TiO_2 nanoparticles coated fibers.

Sample Name	Description
BF	Bare fibers
5PTCF	5% TiO_2 nanoparticles coated fibers
10PTCF	10% TiO_2 nanoparticles coated fibers
15PTCF	15% TiO_2 nanoparticles coated fibers

3.2 Results

3.2.1 Material Characterization of TiO_2 Nanoparticle

The atomic structure TiO_2 nanoparticle used in this study was analyzed via X-ray diffraction study. From the X-ray diffraction pattern below (Figure 3.1), it can be seen that, due to the presence of crystal plans on the material, there is a sharp rise in intensity on (110), (101), (200), (111), (210), (211), and (220) plane. This plane on the material can be attributed to the rutile phase of TiO_2 nanoparticle [87]. The characteristic peaks are seen on the 2θ values of 27.5° and 36.2° corresponding to the (110) and (101) plane of the rutile phase of TiO_2 [84].

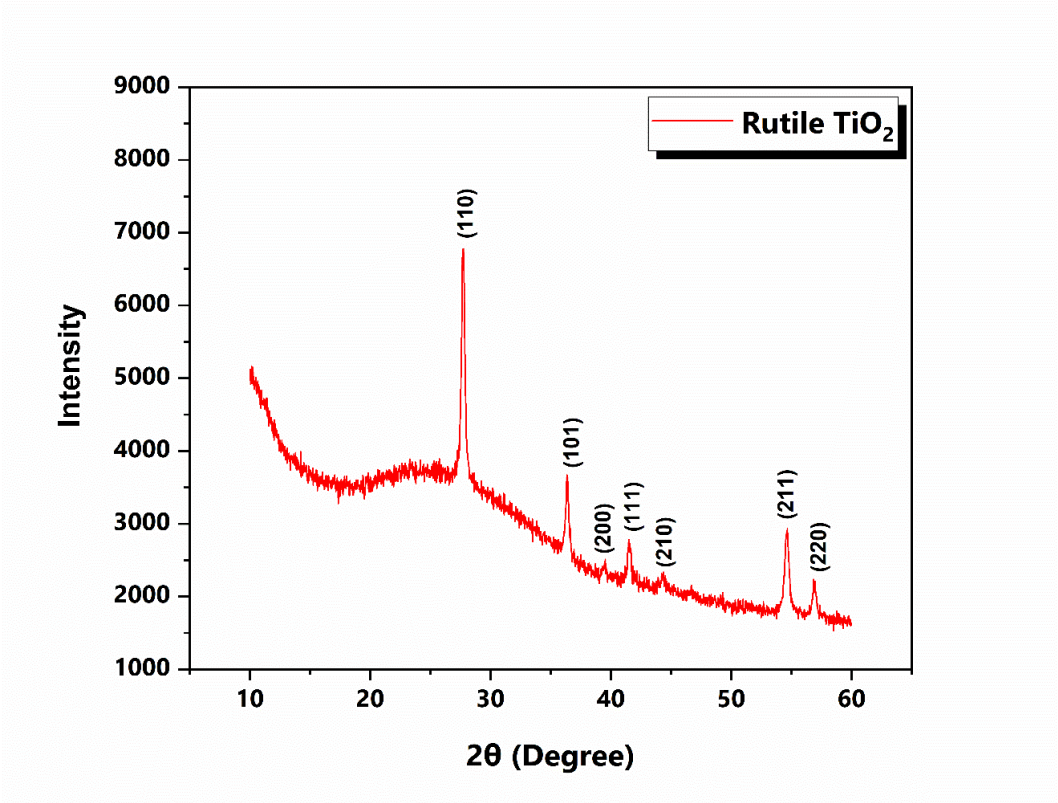

Figure 3.1: XRD pattern TiO_2 nanoparticle deposited on the glass substrate. Characteristics peaks are seen in (110) and (101) planes.

3.2.2 Morphological Characterization

The figure below (Figure 3.2) compares the surface of SEM micrograph nanoparticle-coated fibers and bare fibers. From the images, it can be seen that stabilized nanoparticles are present on the fiber's surface due to bonding by APTES. Moreover, it can also be seen that there exists a correlation between nanoparticle solution concentration and the population of nanoparticles on the fiber surface. It can also be seen that the surface of the GF is almost covered with nanoparticles when the concentration of the solution is 10% TiO_2, and a monolayer of nanoparticles is formed on the surface of the fiber. However, when the concentration was increased to 15% TiO_2, a multilayered coating was observed due to the accumulation of nanoparticles on the fiber's surface (Figure 3.2).

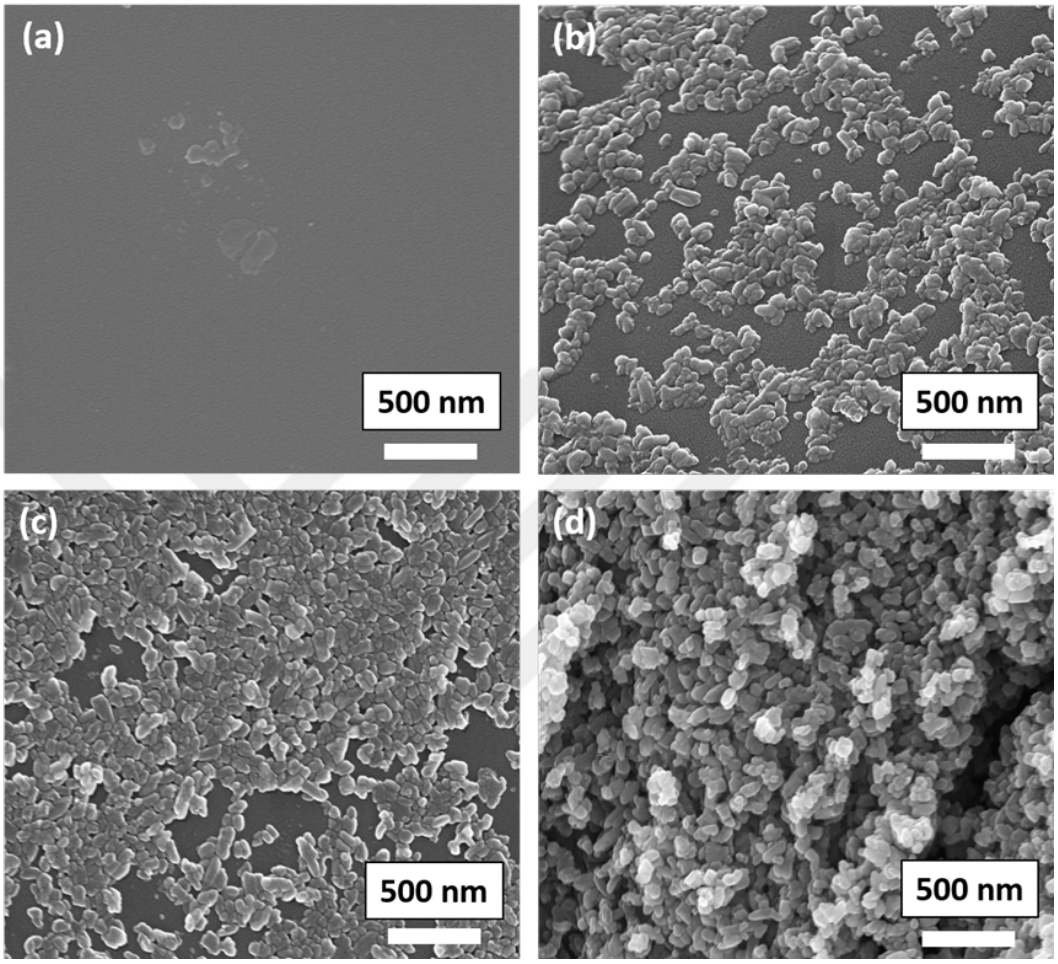

Figure 3.2: SEM images of the glass fiber surface for (a) BF, (b) 5PTCF, (c) 10PTCF, and (d) 15PTCF [19].

The AFM images further proved the presence of nanoparticles on the coated fibers but not on the bare fibers. AFM images (Figure 3.3) also proved the correlation between nanoparticle concentration and the population of nanoparticles present on the surface of the fiber.

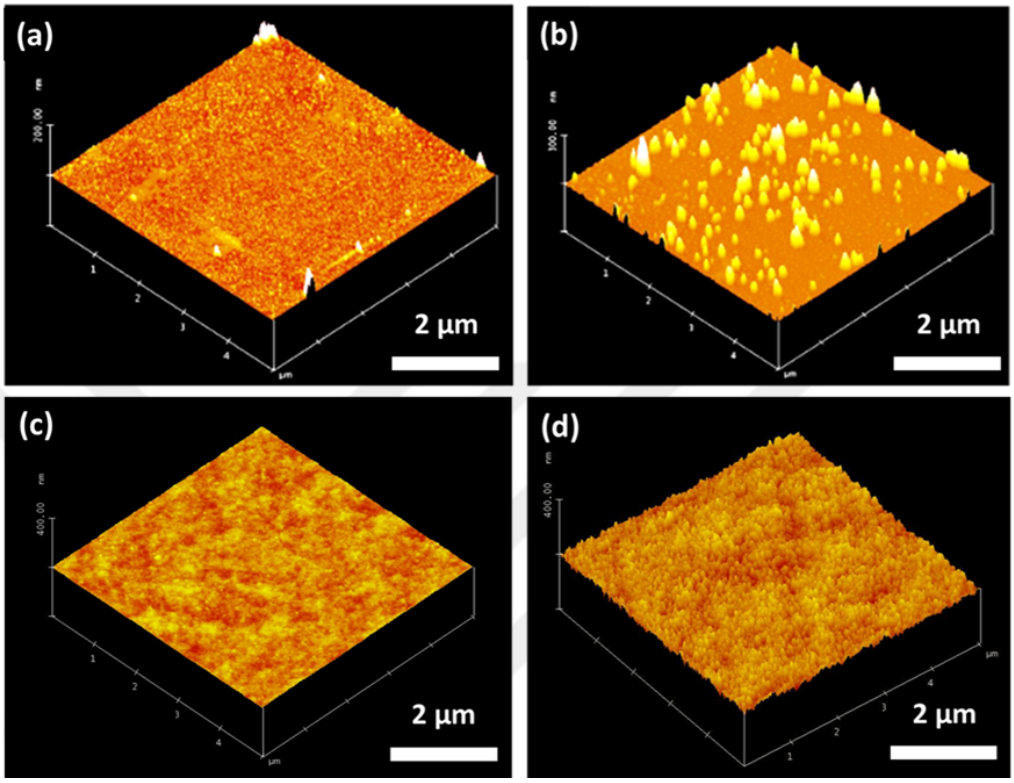

Figure 3.3: AFM images of glass fiber surface for (a) BF, (b) 5PTCF, (c) 10PTCF, (d) 15PTCF [19].

3.2.3 Spectroscopic Analysis

The figure below (Figure 3.4) displays the X-ray photoelectron spectroscopy (XPS) analysis of the coated and uncoated glass fibers. The intensity peak of C1s at 285eV and O1s at 531 eV can be assigned to the functional group present on the GF fiber sizing APTES [20]. Moreover, Ti metal oxide is indicated by the existence of intensity at 458.4 eV and 458.5 eV [85, 86, 87]. Upon a close examination of the energy region between 455 and 475 eV, it can be seen that uncoated fibers exhibit no emission intensity, which demonstrates the absence of Ti metal on the bare fiber surface. However, when 5PTCF, 10PTCF, and 15PTCF fibers were examined, it was found that the emission spectrum's intensity increased with the concentration of nanoparticles. This can be ascribed to the fact that the population of nanoparticles on the fiber surface increased with the nanoparticles'

solution concentrations [88, 89], which is seen from the SEM and AFM images in the previous figures (Figure 3.2 and Figure 3.3).

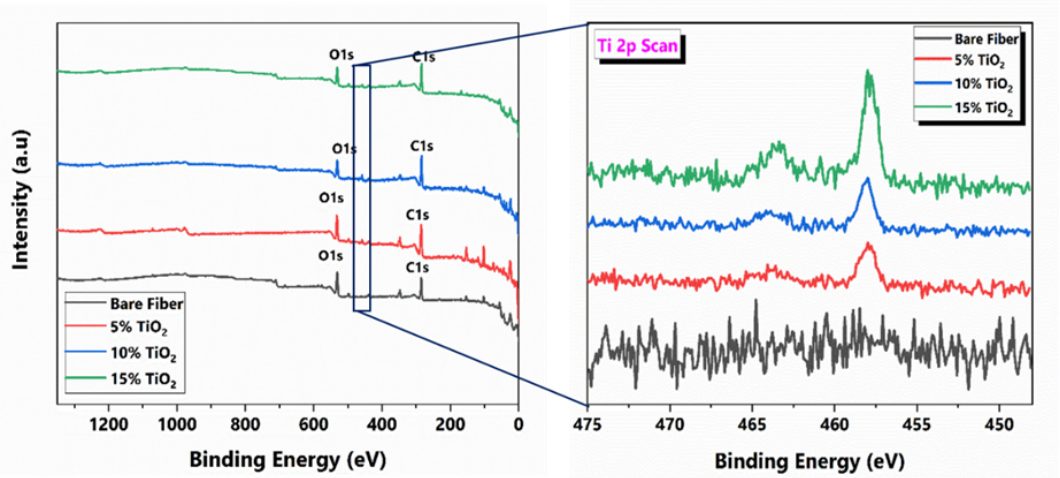

Figure 3.4: XPS spectra of TiO_2 nanoparticles coated fiber surface from 0 to 1350 eV (on the left) and 458 and 475 eV (on the right) [19].

3.2.4 Fractographic Analysis

In order to understand the nature of fracture, a fractographic study was carried out with the SEM. The literature shows that when a surface of fiber fractures by a tensile force, it exhibits three distinct regions: mirror, mist, and hackle region. The following Figure 3.5 shows that the incorporation of TiO_2 nanoparticles on the surface of the fiber did not have any effect on the characteristics regions, where all of the three regions can be clearly seen on the fractured fiber surface [90, 91, 92]. This also means that tensile forces fractured our Glass fiber. Moreover, a correlation between tensile strength and the mirror region of the fiber can be documented. From the figure (Figure 3.5) it can be seen that the tensile strength of the fiber decreases as the mirror region on the fractured surface increases. For instance, it can be deduced from the figure (Figure 3.5) that the mirror region is the smallest for the fiber with the highest tensile strength and vice versa.

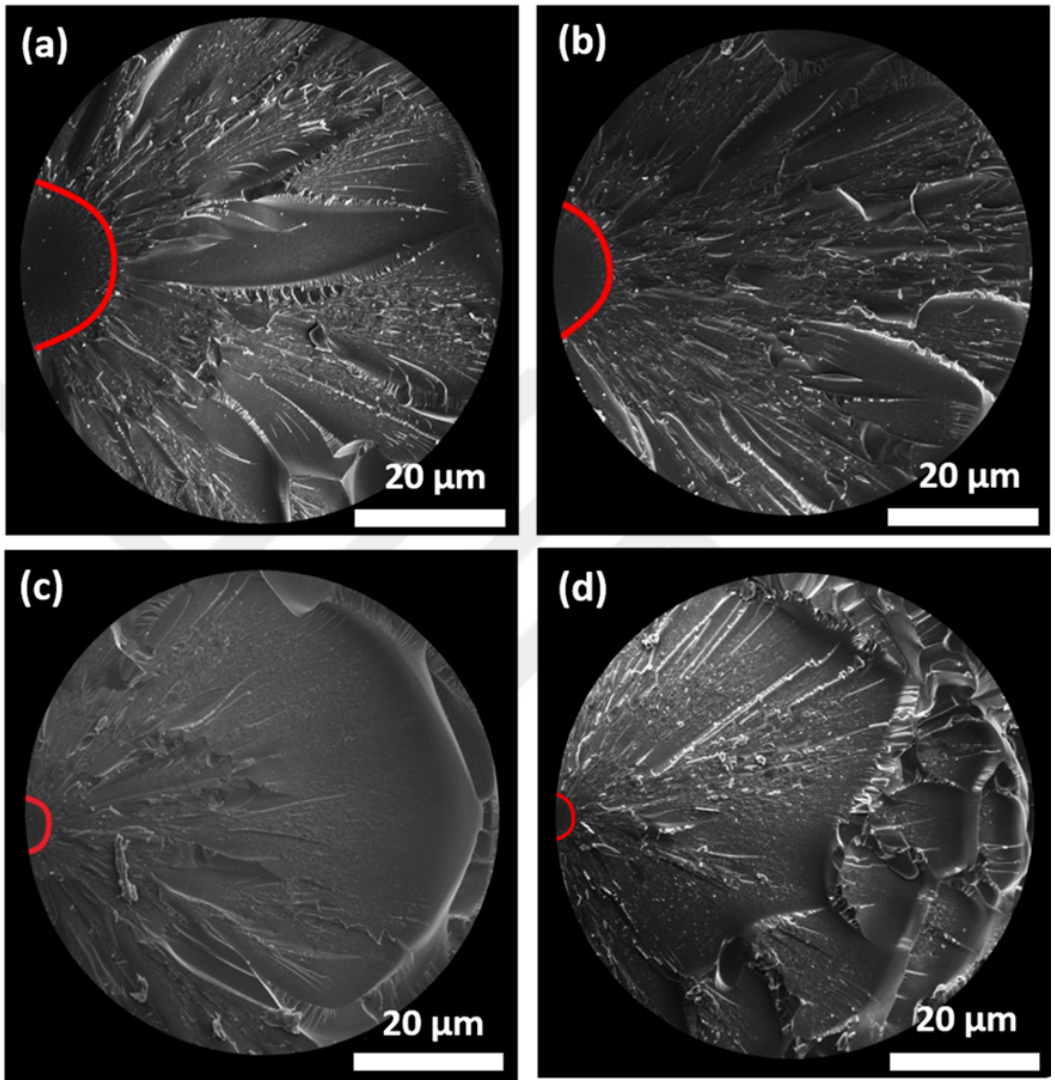

Figure 3.5: Cross-sectional view of the fractured surface placed vertically under the SEM with tensile strengths of (a) 717 MPa, (b) 1012 MPa, (c) 1244 MPa, (d) 1289 MPa [19].

3.2.5 Mechanical Characterization

In order to know the effect of nanoparticles on the mechanical characteristics of the glass fibers, tensile tests were performed both on coated and uncoated glass fibers. It can be understood from the discussion on the morphological analysis that surfaces coating by 5%, 10%, and 15% nanoparticles cover the surface of the glass fiber, and for this reason, it can be said that any possible defects

present on the fiber surface are healed. This can be ascribed to the formation of a polysiloxane network from the interaction of nanoparticle and coupling agent APTES [20, 64]. Additionally, Table 3.2 depicts three distinct subgroups and their tensile strength, standard error, and Weibull modulus with respect to different concentrations of nanoparticles. In order to increase the reliability of the data, around 50 to 60 fibers were studied. Nearly 50% of those fibers broke at the edge or slipped, and these fibers were omitted from the study. The rest of the fibers were considered for the final calculation. It may seem that the same types of fibers have different tensile strengths. However, as we know, the tensile strength of fibers also depends upon the surrounding atmosphere, and since the experiments were performed on different days, they experienced different conditions, which is why the difference in the tensile strength of the glass fibers [93]. The figure on the next page (Figure 3.6) compares the tensile strength and probability of failure at certain stress of bare fibers and TiO_2 (5%, 10%, and 15%) nanoparticles coated fibers on glass fiber.

From Figure 3.6, it can be seen that nanoparticle coating has improved the Weibull modulus for all of the mentioned three cases. This indicates that nanoparticle-coated fibers are less likely to fail at a given strength compared to bare fibers. Combining information from, Table 3.2 and Figure 3.6, it is shown that 5PTCF mean tensile strength stands at 778 MPa with a Weibull moduli 2.30, as opposed to the BF, which exhibit a mean tensile strength of 725 MPa with a Weibull modulus of 2.56. This means that 5% TiO_2 nanoparticle coating has improved the tensile strength by 7.31% . In addition, when fibers were dip-coated using 10% TiO_2 nanoparticle solutions, bare fibers, and nanoparticle-coated fibers demonstrated a tensile strength of 862 MPa and 963 MPa, respectively, which is actually an 11.71% increase in the tensile strength. Besides, the Weibull moduli also improved to about 73% reaching a value of 5.60 from 3.24. Finally, in the last group, 15PTCF has a tensile strength of 816 MPa, while the BF shows a strength of 744 MPa. This resulted in an improvement of 9.67% tensile strength of glass fiber. Moreover, the Weibull modulus reached 3.46 from 2.67, meaning that the probability of the failure of the fiber under certain stress has decreased. The improvement in tensile strength and lower probability of failure of glass fibers

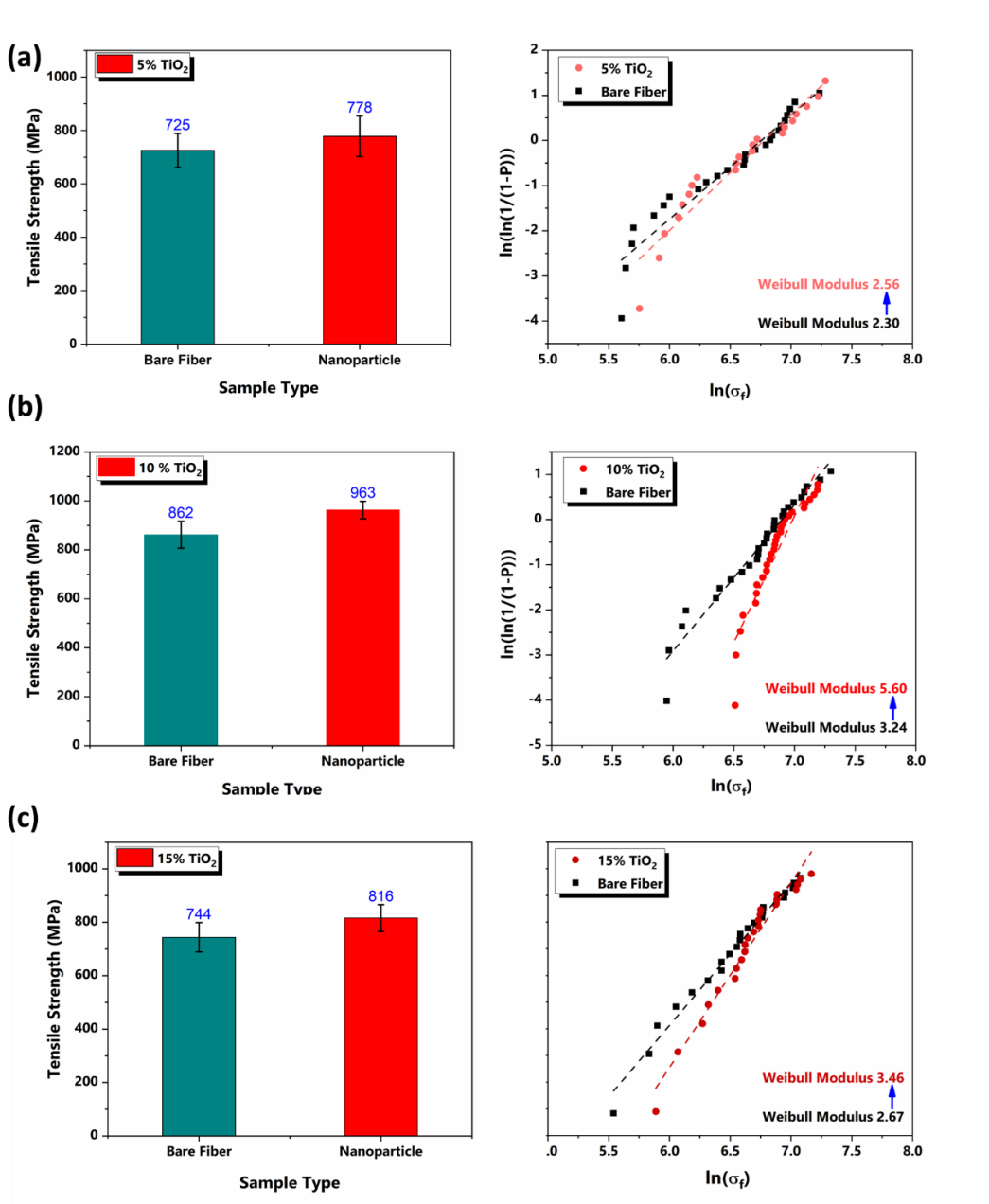

Figure 3.6: Comparison of tensile strength and Weibull modulus of three-subgroup fibers (a) 5PTCF (b) 10PTCF and (c) 15PTCF. All of them were compared with respect to bare fibers. The standard error is shown as the error bar [19].

have happened due to the delayed propagation of cracks owing to nanoparticle coatings making a rough surface [22].

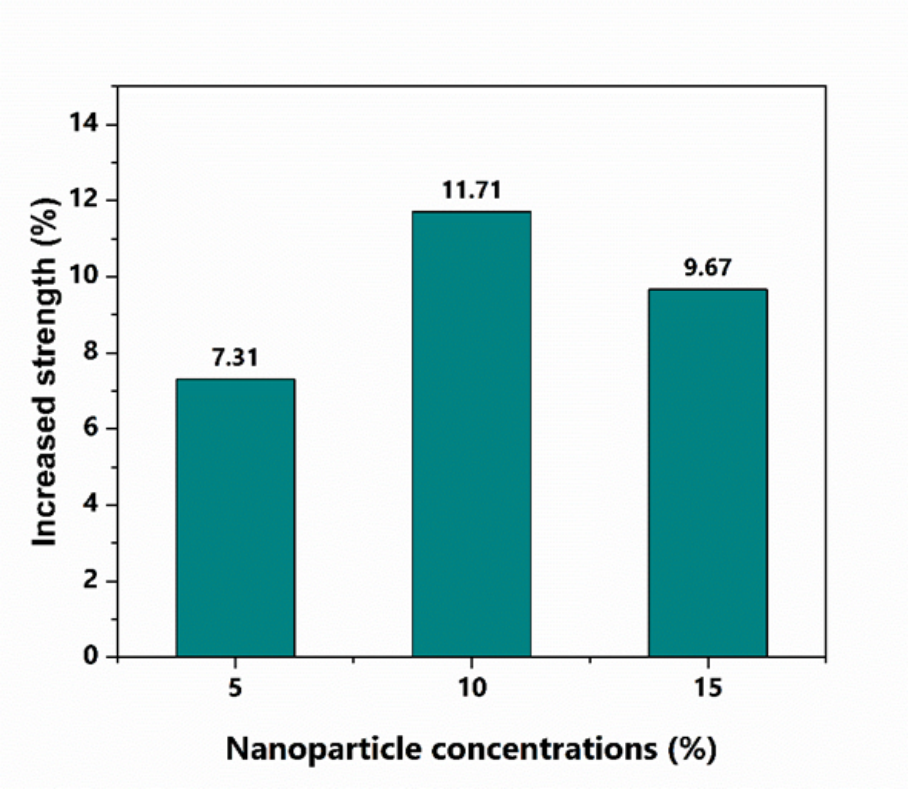

Figure 3.7: Effect of TiO_2 nanoparticles coating on the tensile strength of glass fibers [19].

The tensile strength improvement in the glass fiber as a function of nanoparticle concentration is summarized in Figure 3.7. It can be seen that, although there might be a difference in the proportion of the increase in the tensile strength, it is enhanced for every concentration. A more detailed inspection of the results shows that tensile strength is mostly improved for the 10PTCF, and 15PTCF has lower improvement as opposed to 10PTCF but superior to 5PTCF. This may happened due to the formation of microvoids on the surface of glass fibers due to the existence of higher concentrations of coagulated nanoparticles presence on the fiber surface [74]. SEM images Figure 3.2(d), AFM images Figure 3.3 (d), and XPS Spectra (Figure 3.4) further confirm the development of microvoids on the fiber surface. Microvoids hinder the stress propagation on the fibers causing an accumulation of stress on the fiber, thus causing the failure of the tensile-strength

glass fiber [74].

Table 3.2: Mean tensile strength, standard error, and Weibull modulus for the three subgroups of fibers. Different shades in the table represent different subgroups. Around 180 fibers were taken for the final calculation for six subgroups of fibers [19].

Subgroups	Tensile Strength (MPa)	Standard Error	Weibull Modulus (m)
Bare fiber	725	± 64	2.30
5% TiO_2 coated fiber	778	± 76	2.56
Bare fiber	862	± 55	3.24
10% TiO_2 coated fiber	963	± 36	5.60
Bare fiber	744	± 55	2.67
15% TiO_2 coated fiber	816	± 50	3.46

3.3 Conclusions

This chapter examined a morphological, mechanical, and statistical analysis of Glass fibers after coating them with varied concentrations of TiO_2 nanoparticle solutions. For this reason, nanoparticle solutions of different concentrations were dip-coated on the E-glass fiber surface. Morphological and spectroscopic analyses provided proof that nanoparticles are present on the fiber surface. Weibull analyses were also employed to statistically analyze the fibers' strength and failure probability. It showed that, in all the cases, TiO_2 nanoparticle-coated fibers have a lower probability of failure than bare fibers, and it also exhibits higher strength than bare fibers. It is also reported that the tensile strength of single glass fibers can be increased by up to 11.7% with a 10% TiO_2 nanoparticles solution coating. From the fractographic analysis, it was also demonstrated that, fiber is fractured by tensile force, and a correlation exists between fractured surface's mirror region and tensile strength.

Chapter 4

Silica and Zirconia Nanoparticle-coated Fibers

4.1 Introduction

In fiber-based composites, glass fibers (GFs) are the most frequently employed reinforcement materials owing to their excellent performance while maintaining a moderate cost [20, 83, 94, 95]. Moreover, it is vital to consider the fibers' chemical resistance against the alkaline solution to expand the usage of the fiber as a structural element. This property of chemical resistance becomes vital when the fibers are exposed to alkaline conditions in sewage pipes, boats, and structural concretes [96, 97]. Although there already exist glass fibers that are resistant to alkaline solutions are known as AR glass fibers. Around 15-23% of ZrO_2 nanoparticles are found in the AR glass fiber as a chemical constitute [98]. A significant component of AR resistance glass fibers is zirconia (ZrO_2), and due to its high bonding energy, it provides resistance in alkaline conditions. However, the production cost of AR glass fibers is very high owing to the very high melting temperature and the complexity of manufacturing [99] [103]. On top of that, it is very difficult to fiberize AR glass fiber as it has very high viscosity [100]. Coating of E-glass fibers via zirconia (ZrO_2) nanoparticles is a promising alternative solution to overcome

the problems associated with high-energy consumption, viscosity, and material cost.

In this chapter, the effect of amorphous SiO_2 nanoparticles (diameter 8-33 nm) coating on the mechanical properties of E-glass fibers are investigated. Then, the impact of monoclinic ZrO_2 (diameter 40-50 nm) coating on the chemical characteristics of E-glass fibers is also analyzed via morphological and surface analysis. Additionally, the mechanical behavior of nanoparticle-coated fibers is investigated by the Weibull statistics.

Table 4.1: Naming conventions used for studying the effect of SiO_2 and ZrO_2 nanoparticles coating on glass fibers.

Sample Name	Description
BF	Bare fiber
5PSCF	5% SiO_2 nanoparticles coated fibers
10PSCF	10% SiO_2 nanoparticles coated fibers
15PSCF	15% SiO_2 nanoparticles coated fibers
A-BF	Aged bare fibers
A-ZCF	Aged ZrO_2 nanoparticles coated fibers
5PZCF	5% ZrO_2 nanoparticles coated fibers
10PZCF	10% ZrO_2 nanoparticles coated fibers

4.2 Results and Discussion

4.2.1 Material Characterization of SiO_2 Nanoparticle

In order to know the crystal structure of our materials the materials were subjected to X-ray diffraction (XRD) study. The figure below shows the XRD results of the SiO_2 nanoparticles used in this study. From Figure 4.1, it can be seen that there is no sharp intensity peak on the spectrum, meaning that the material does not have any constructive interference due to the absence of a well-defined plane

on the materials. For this reason, SiO_2 materials used in this study can be defined amorphous [101].

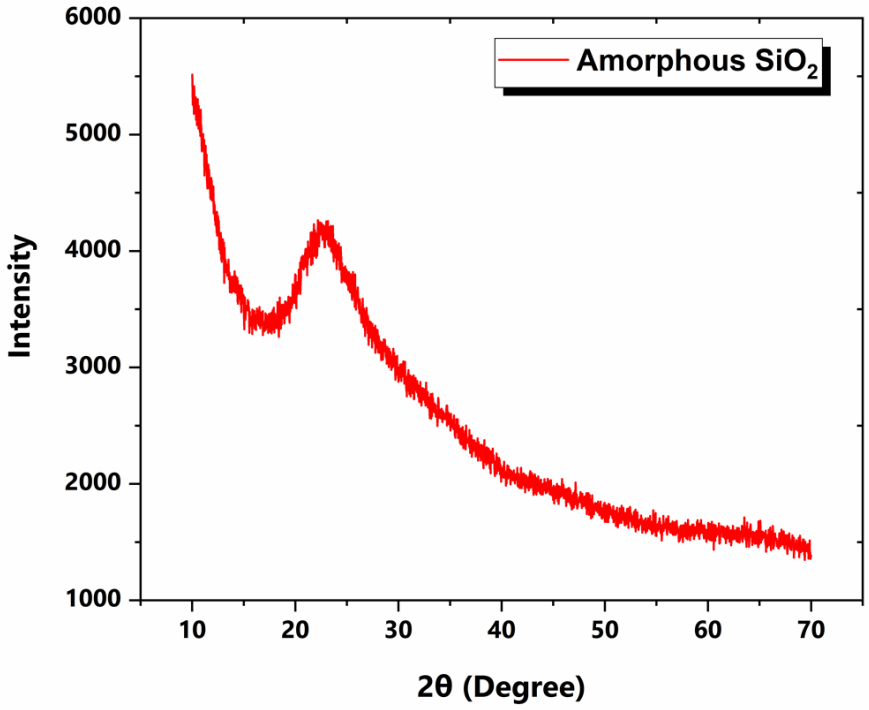

Figure 4.1: XRD pattern SiO_2 nanoparticle deposited on the glass substrate. There is no sharp peak due to the absence of crystallinity on the material.

4.2.2 Materials Characterization of ZrO_2 Nanoparticle

In this section, the crystal structure of the ZrO_2 nanomaterials was investigated. Contrary to the SiO_2, this material has demonstrated very sharp intensities due to the crystal plane on the materials. From the XRD pattern (Figure 4.2), it can be seen that the materials exhibit sharp intensities on (001), (110), (011), (-111), (111), (200), (022), (120), (-112), (211), (220), (022), (220), (310), (131), (113), and (222). This plane in the figure corresponds to the monoclinic nature of the material [102]. The major peak of this spectrum was at (-111), (111), (022), (131) plane which corresponds to 2 values of 28.2°, 31.5°, 50.1°, and 59.8° respectively,

and this can be attributed to the monoclinic phase of ZrO_2 [103, 104].

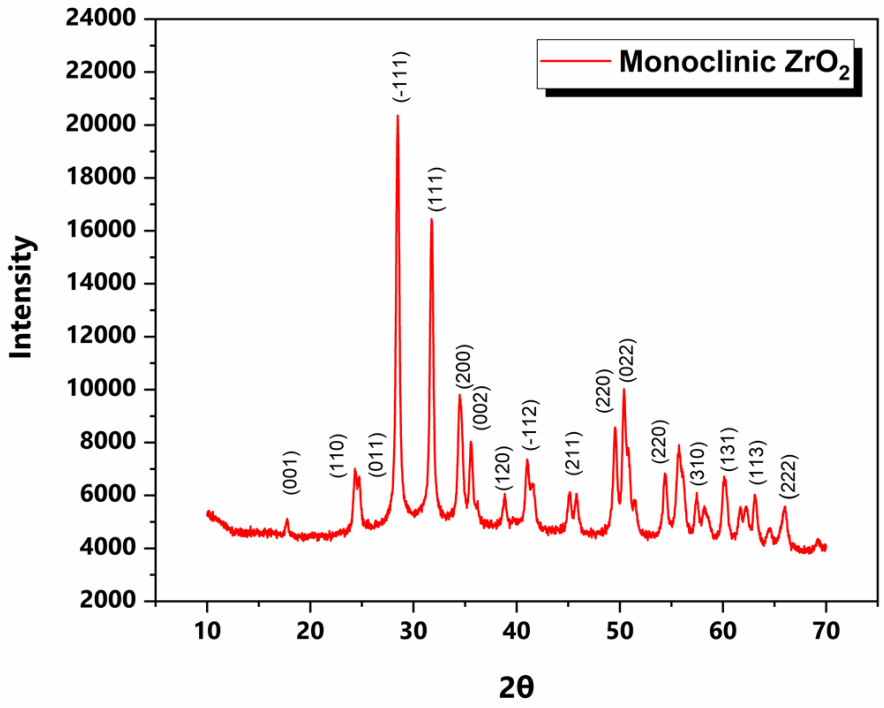

Figure 4.2: XRD pattern ZrO_2 nanoparticle deposited on the glass substrate. Characteristics peaks are seen on (-111), (111), (022), and (131) planes.

4.2.3 Morphological Characterization of SiO_2 Nanoparticles-coated Fiber

The figure below (Figure 4.3) provides information about the morphological characteristics of the SiO_2 nanoparticle-coated glass fiber surface. From Figure 4.4 (a), (c), and (e), we can see that surface of the nanoparticle-coated glass fiber is non-uniform, and fractured. Figure 4.3 (b), (d), and (f) is magnified images of the previous three figures, which clearly show the glass fiber surface coated with SiO_2 nanoparticles is fractured, and we can see a fractured shell on the surface of the glass fiber. This may happen due to the amorphous nature of nanoparticles (Figure 4.1). However, further analysis is necessary to come to an unambiguous

decision.

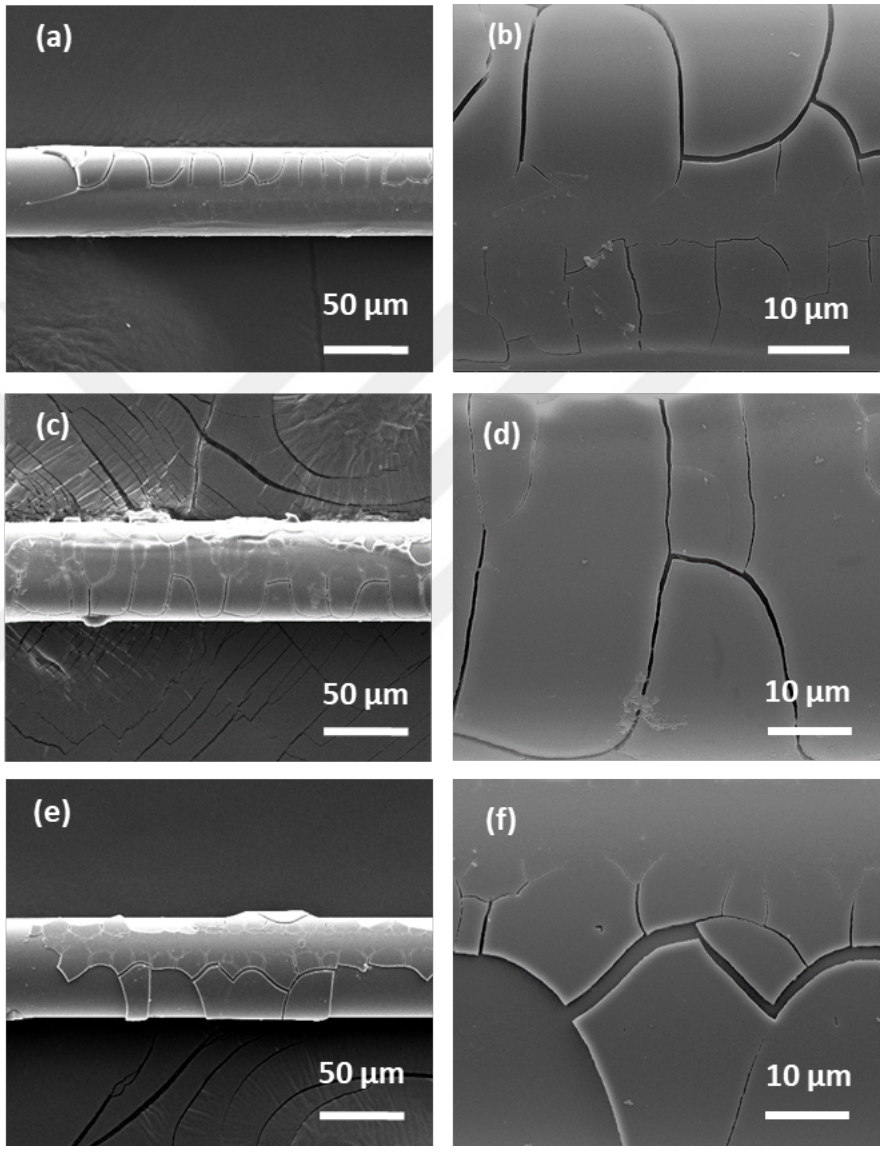

Figure 4.3: SEM images of the fiber surfaces after coating with (a) 5PSCF, (b) 5x magnified image 5PSCF, (c) 10PSCF, (d) 5x magnified image of 10PSCF, (e) 15PSCF, and (f) 5x magnified image of 15PSCF.

4.2.4 Morphological Characterization of ZrO_2 Nanoparticles-coated Fiber

The following figure (Figure 4.4) shows the SEM micrographs of the bare and ZrO_2 (5%, 10%, and 15%) nanoparticles coated E-glass fibers. Previous research on this area says that when ZrO_2 is exposed to SiO_2 glass fibers, due to the interaction of Zr to the Si, it forms Zr-O-Si chemical bond and remains on the fiber's surface [105, 106]. Additionally, a correlation between nanoparticle concentration and the population of nanoparticles present on the fiber surface can also be observed—the higher the concentration of nanoparticles, the higher the population of nanoparticles on the glass fiber surface. A close inspection of the glass fiber surface shows that 5PZCF is nearly half covered by the ZrO_2 nanoparticle, as the uncovered glass fiber surface can also be noticed. The 10PZCF fibers are almost fully covered, and only very few uncovered areas can be observed on the fiber surface. Additionally, for the 15PZCF, no uncovered region is observed under the SEM, suggesting uniform coating over the fiber surface.

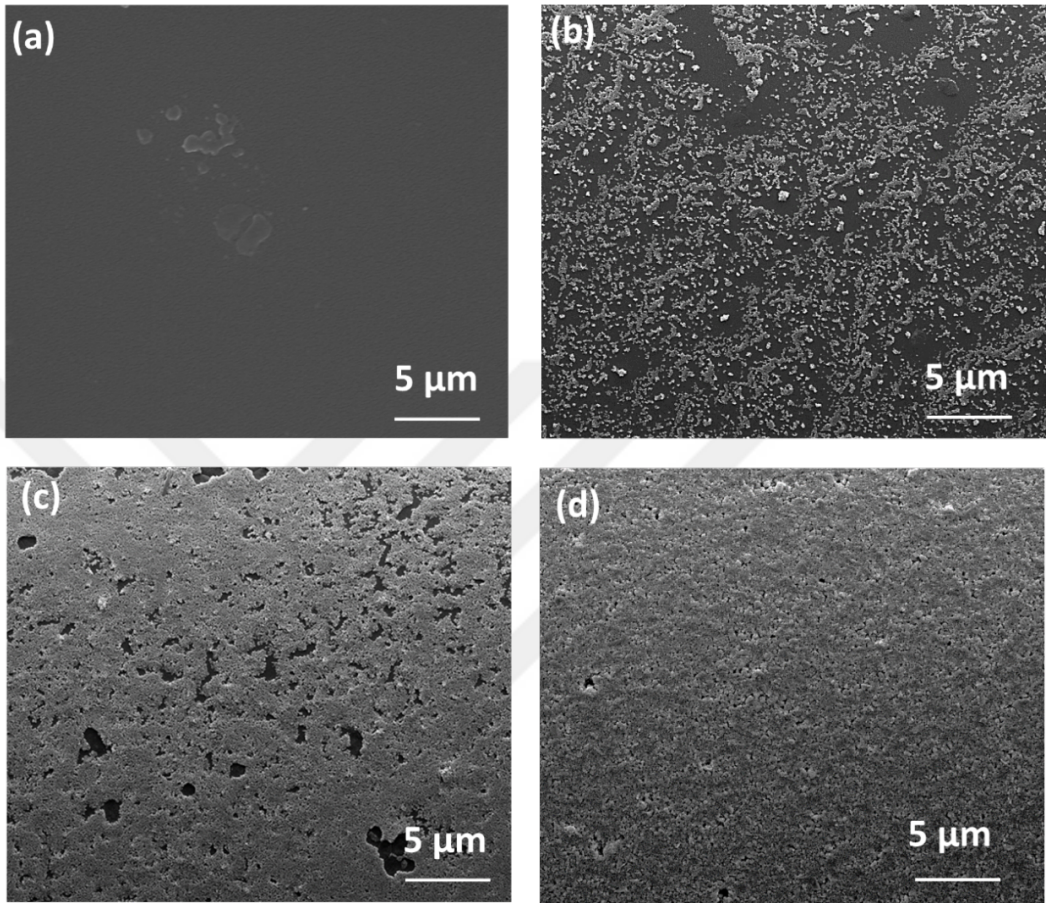

Figure 4.4: SEM micrographs show the surface of the glass after coating (a) Bare Fiber, (b) 5PZCF, (c) 10PZCF, (d) 15PZCF.

4.2.5 Mechanical Characterization of SiO_2 Nanoparticles-coated Fibers

After the material characterization and morphological analysis, a tensile test was run on bare and nanoparticle-coated fiber to see the impact of 5%, 10%, and 15% SiO_2 nanoparticle coating on the mechanical properties of E-glass fibers. The figure shows that 5%, 10%, and 15% SiO_2 nanoparticles coating of fibers have decreased the tensile test of glass fibers by 7.64%, 10.64%, and 13.4% (Figure 4.5 and Figure 4.6). However, the Weibull modulus was increased for 5PSCF and 15PSCF and decreased for 10PSCF (Figure 4.5). The surface morphology of nanoparticle-coated fibers can explain the reason for the decrease. When we

look at the surface of SiO_2 nanoparticles coated E-glass fibers, we can see that the surface is fractured even before the fiber is subjected to tensile force by the micromechanical analyzer (Figure 4.3).

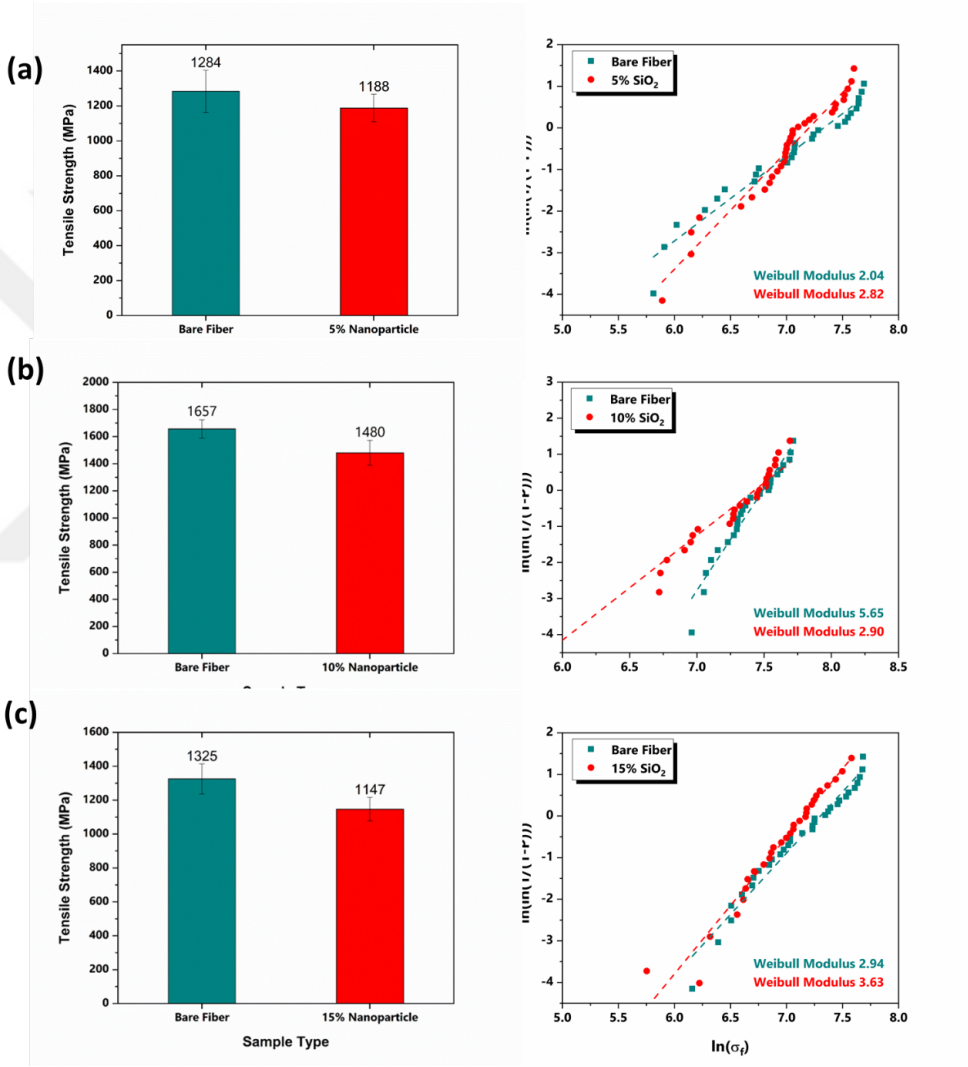

Figure 4.5: Tensile strength and Weibull distribution of (a) 5PSCF, (b) 10PSCF, and (c) 15PSCF. All of the nanoparticle-coated fibers are compared with respect to bare fibers. The standard error is shown as the error bar.

Moreover, from the literature, we know that the material's surface must be uniform and homogeneous to transfer the stress applied via tensile force [14, 15]. On the contrary, for this set of samples from the SEM inspection, it was observed the SiO_2 nanoparticles coated glass fibers surface are non-uniform and even fractured. The non-uniform surface of glass fibers does not allow the stress applied

via the micromechanical analyzer to dissipate. Additionally, from the Griffith theorem, we also know that surface defects on the fibers act as a stress accumulator. For this reason, the SiO_2-coated glass fibers are losing tensile strength [56].

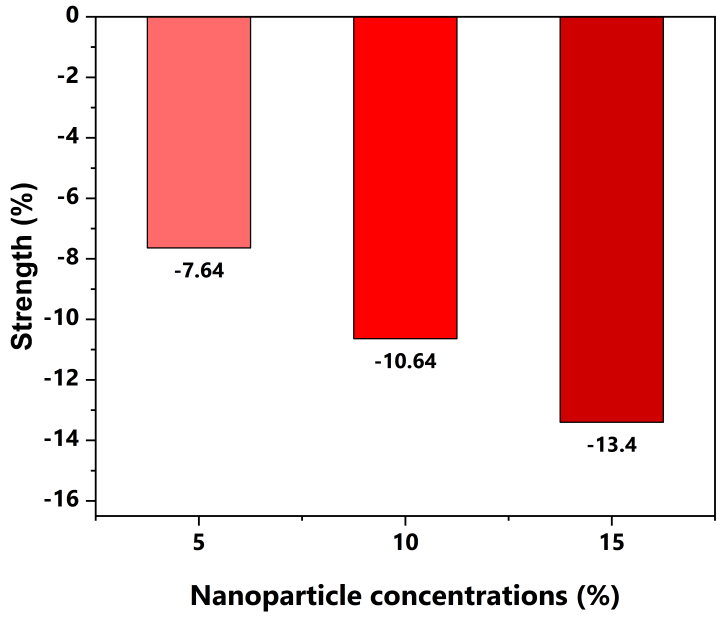

Figure 4.6: Effect of SiO_2 nanoparticles coating on the tensile strength of glass fibers.

4.2.6 Analysis of Fractured Fiber

In order to investigate the reason for the fracture, we also carried out a further stepwise analysis of the fractured fiber to know when the fiber is fractured. For this reason, the 10PSCF are observed under the scanning electron microscope for four steps and compared with the as-received fiber surface. The figure (Figure 4.7) shows that the surface of the as-received fibers doesn't contain any visible fracture. However, just after coating them with amorphous SiO_2 nanoparticles, non-uniform and fractured surfaces of glass fiber can be observed. It is also seen that fractured shells are also present on the fiber surface after the first annealing on the furnace and the second annealing after the silanization process. This

means the same fractured surface is continued upon all these steps, and even silanization was not enough to heal the surface defects of that large. This figure shows that the fracture happens because of the coating, not with the annealing or other actions.

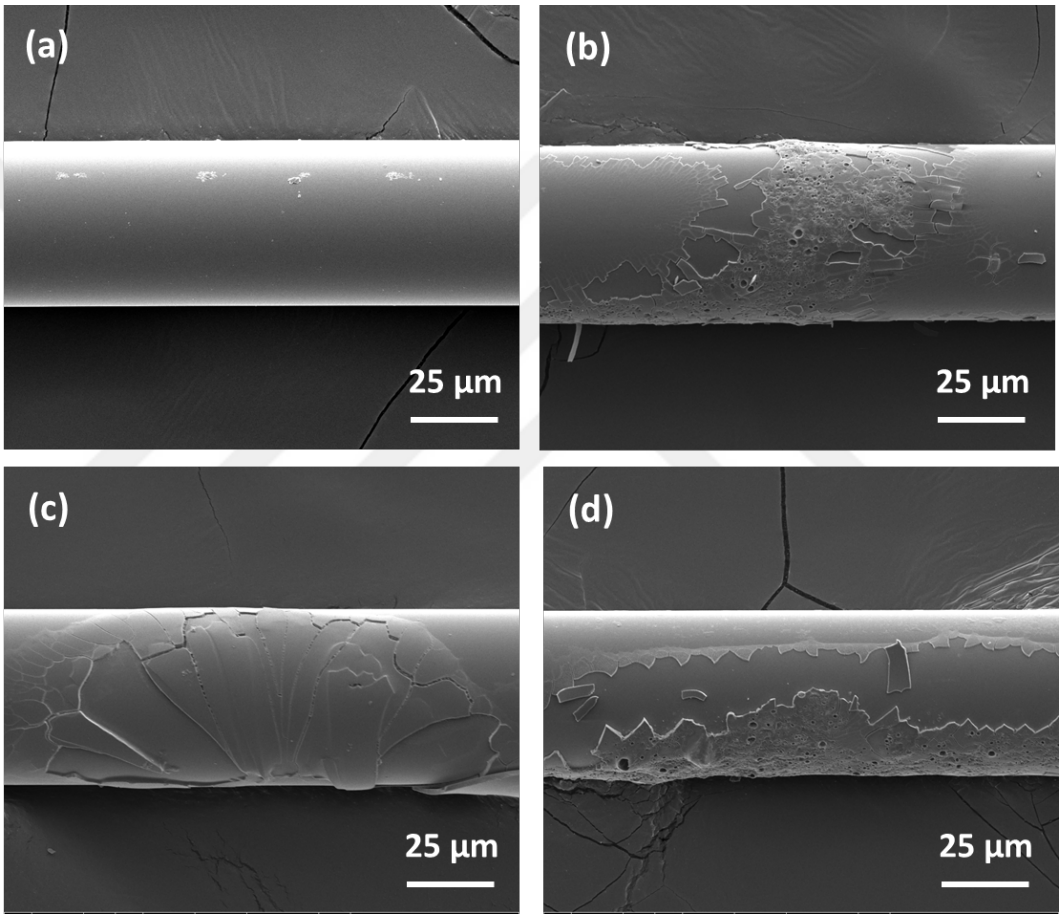

Figure 4.7: Stepwise analysis of SiO_2 nanoparticles coated fiber (a) As received fiber, (b) 10% SiO_2 nanoparticles coated fiber, (c) 10% SiO_2 nanoparticles coated fiber after the first annealing process without silane, (d) 10% SiO_2 nanoparticles coated fiber after the second annealing process with silane.

Although we were certain that this fractured surface was due to an amorphous SiO_2 nanomaterials solution, observing the nanoparticle with scanning electron microscopy was not possible. In order to prove the fractured materials on the glass fiber surface, In the next process, a layer of fiber was mechanically peeled on the carbon tape to analyze the chemical composition via the energy dispersive x-ray (EDX) of SEM. Figure 4.8 (a) shows the peeled fiber surface, and Figure 4.8 (b)

shows the elemental composition of the fiber surface. From the elemental analysis, it can be seen that the peeled fiber surface only contains emission intensity from Si and O elements [107]; these elements resulted from the coating we applied via the dip-coating method. This further confirms that fractured surface on glass fibers are due to the coating of SiO_2 nanoparticles.

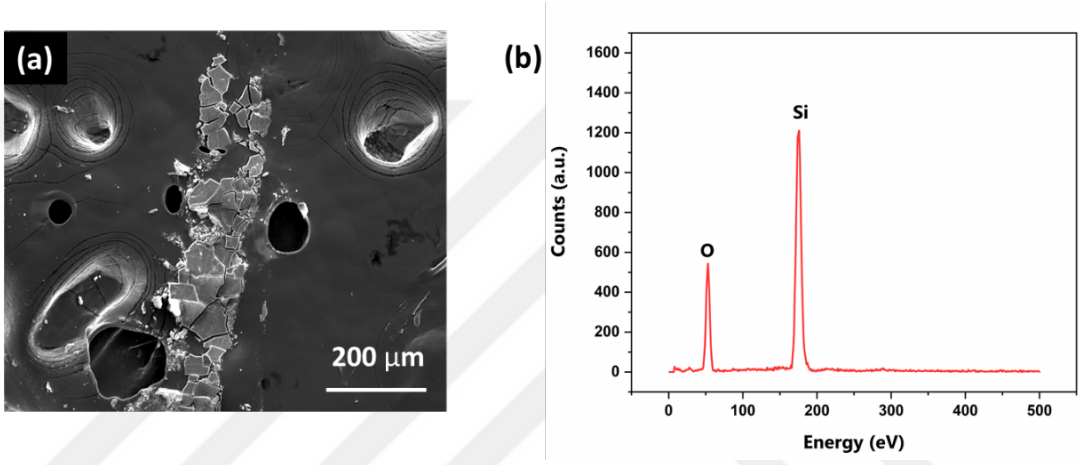

Figure 4.8: Compositional analysis of the peeled surface of nanoparticle coated fiber, (a) peeled fiber surface, (b) elemental composition of the peeled surface via energy dispersive X-ray study.

4.2.7 Mechanical Characterization of ZrO_2 Nanoparticles-coated Fibers

Just like the previous method, ZrO_2 nanoparticle-coated E-glass fibers were investigated with a micromechanical analyzer. After the morphological analysis, a tensile test was run on bare and nanoparticle-coated fiber to see the impact of 5% and 10% nanoparticle coating on the mechanical properties of E-glass fibers. From Figure 4.9, it can be seen that bare fibers have different tensile strength values on different days. However, different nanoparticle concentrations were coated on different days, and the test was conducted on different days. On those days, humidity, temperature, and exposure of the same fibers were different, and this resulted in a mismatch of tensile strength values [56, 93].

From the graph (Figure 4.9 and Figure 4.10) it can be observed that zirconia

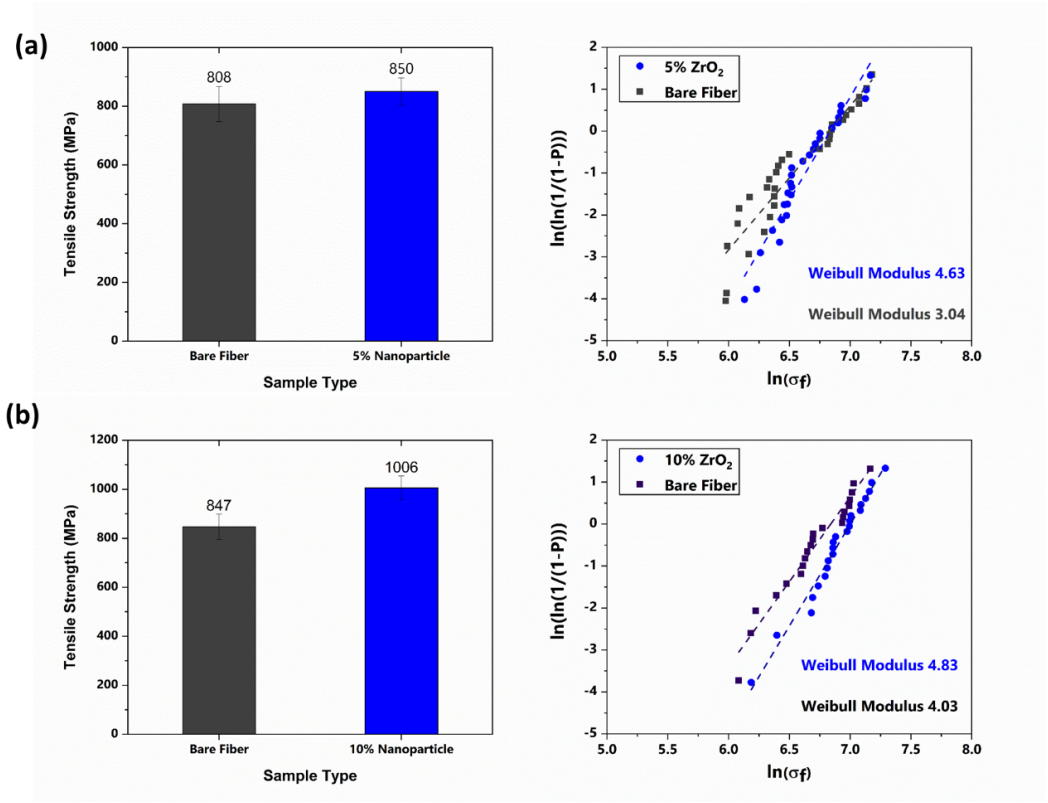

Figure 4.9: Tensile strength of bare fibers and zirconia-coated fibers (a) 5PZCF, (b) 10PZCF. The Standard error is shown as the error bar.

nanoparticle coating has improved the tensile strength of glass fibers in both the cases 5PZCF and 10PZCF. Besides, it can also be seen that nanoparticle-coated fibers have a higher Weibull modulus compared to bare fibers. Since the Weibull modulus is increased, meaning the scatter of the data has reduced, and thereby nanoparticle coating has contributed to making uniform healed fiber surface. The higher strength of nanoparticle-coated fibers means nanoparticles are able to suppress crack propagation on the surface of glass fibers.

4.2.8 Testing of Glass Fibers in Alkaline Solutions

The following (Figure 4.11) depicts the effect of surface aging of bare fiber, 5% 10% and 15% nanoparticle-coated glass fibers. From the figure, it is very clear that bare fiber was exclusively corroded when it was exposed to alkaline solutions

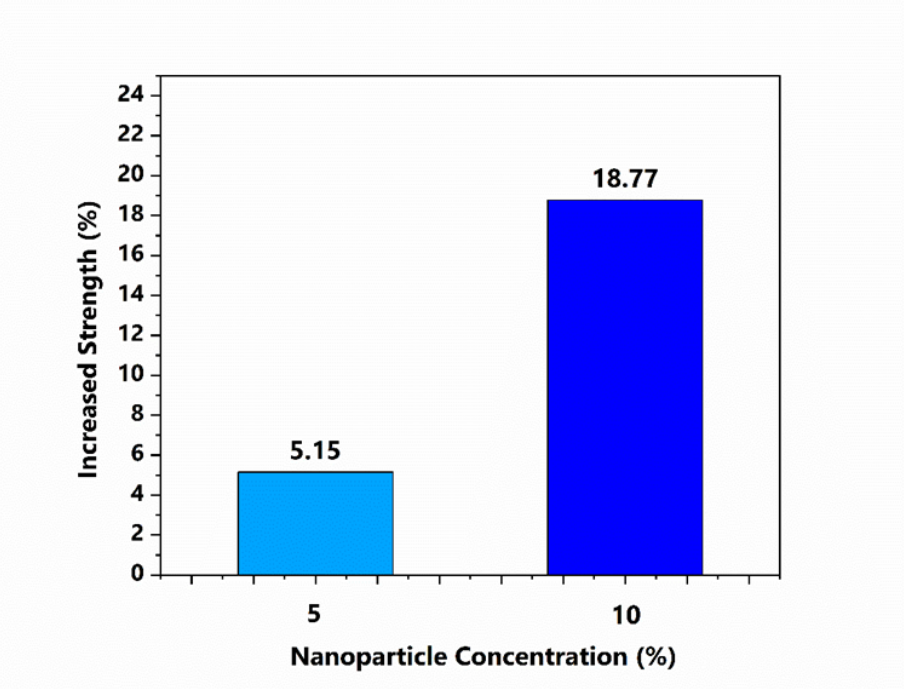

Figure 4.10: Effect of ZrO_2 nanoparticles coating on the tensile strength of glass fibers.

for 4 days. The corrosion results from the attack of the hydroxyl ion of NaOH to the Si-O-Si bond, thereby releasing silicates into the solution [96, 108]. Presence of an alkaline medium such as NaOH dissolves the SiO_2 network of the glass fiber. It can be chemically written by the following formula.

$$\equiv Si - O - Si \equiv + \ OH^- \rightarrow \equiv Si - OH + \equiv Si - O -$$

From Figure 4.11, it can also be observed that a correlation exists between the intensity of corrosion and the concentration of nanoparticles. Although a corroded fiber surface is observed in Figure 4.11-(c) for the 10PZCF due to the non-uniform coating of glass fiber, this amount is highly minimized for 15PZCF due to the uniform coating of nanoparticles before aging Figure 4.11-(d).

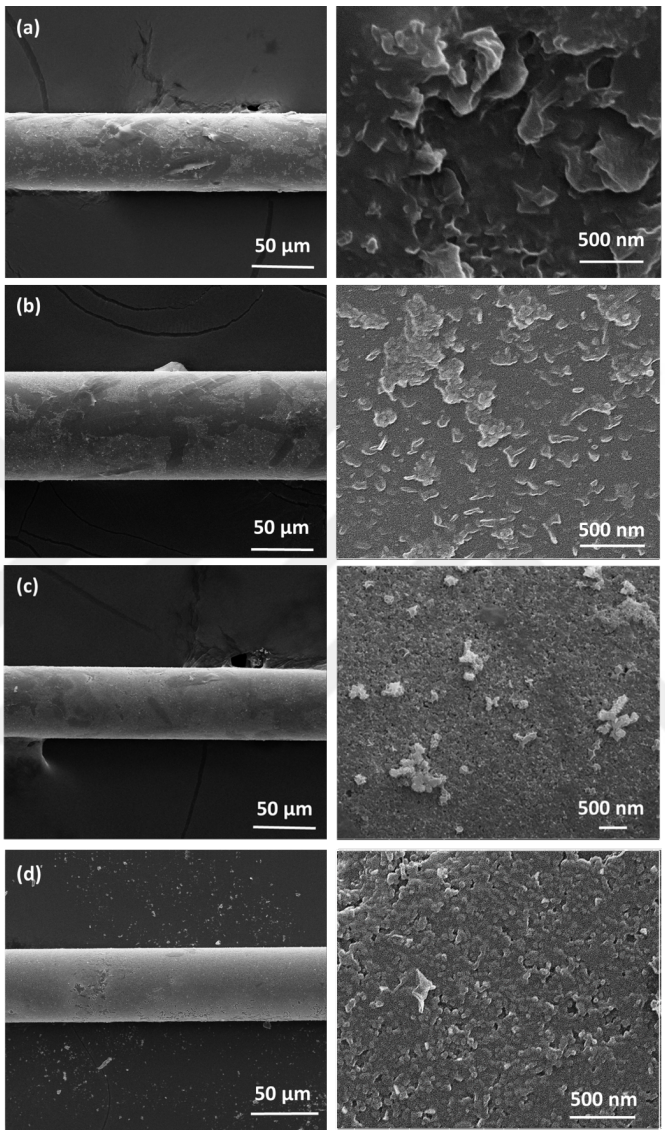

Figure 4.11: SEM images of the fiber surface for (a) A-BF, (b) A-5PZCF, (c) A-10PZCF, and (d) A-15PZCF for 4 days of aging (dwelling) in alkali solution.

4.2.9 Elemental and Compositional Analysis of Glass Fibers

Figure 4.12 depicts the compositional analysis of aged bare fibers and 15% nanoparticle-coated fibers after dwelling in NaOH alkaline (pH 13.5) for four days. Figure 4.12 (a) shows the main elemental compositions O, Na, Mg, Al, Si,

and Ca present on the glass fibers [3, 109]. Figure 4.12 (b), which is 15PZCF aged for 4 days in NaOH solution, shows all the major elements with additional element Zr in energy band 2.042 eV that resulted from the coated surface (Figure 4.4). The presence of Zr validates the claim that was made previously from the SEM images in Figure 4.11 that 15PZCF contains Zr even after dwelling in alkaline solutions for 4 days.

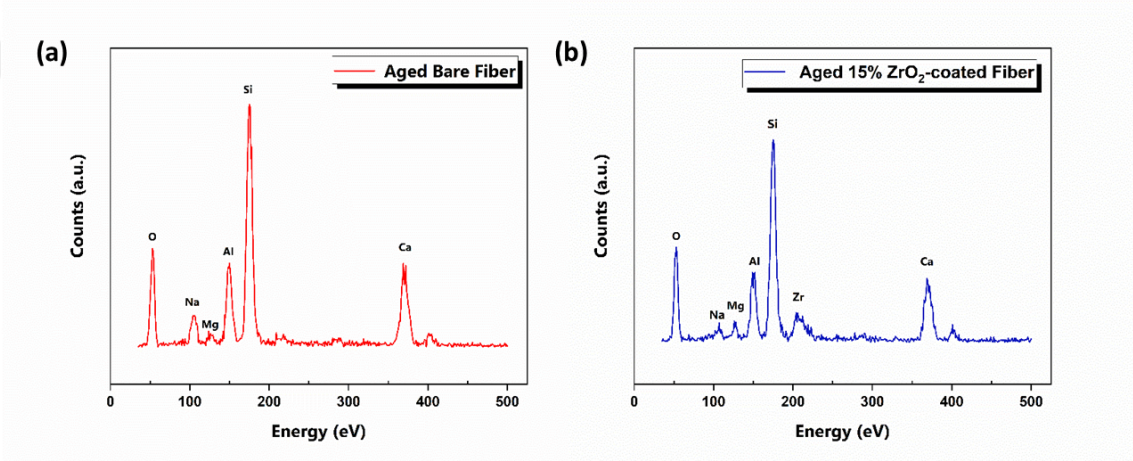

Figure 4.12: Energy-dispersive spectroscopic analysis of selected (a) A-BF and (b) A-15PZCF after 4 days of aging (dwelling) in an alkali solution.

In the next process, compositional analysis was done on bare fibers and 15% ZrO_2 coated fibers (15PZCF) to see the change in the atomic weight percentage of the materials with the help of energy dispersive X-ray study of SEM before and after dwelling in alkaline solutions (pH 13.5) for 4 days. The following graph (Figure 4.13), shows the atomic weight percentage of the major constitutional element, Si, O, Ca, and Zr in bare fibers (BF), aged bare fibers (A-BF), and 15% ZrO_2 coated fibers (15PZCF), and aged 15% ZrO_2 coated fibers (A-15PZCF) calculated from the energy dispersive X-ray study of SEM.

From the figure (Figure 4.13) we can see that there is a sharp drop in the atomic weight percentage of Silicon (Si) in the A-BF after 4 days of dwelling in the alkaline solution. This decrease happens due to the release of silicates onto the solution as an attack of hydroxyl ions from the alkaline solution [101], [112]. However, when we compare the same Si proportion in 15PZCF and A-15PZCF, we see the atomic weight percentage of Si remained the same even after 4 days

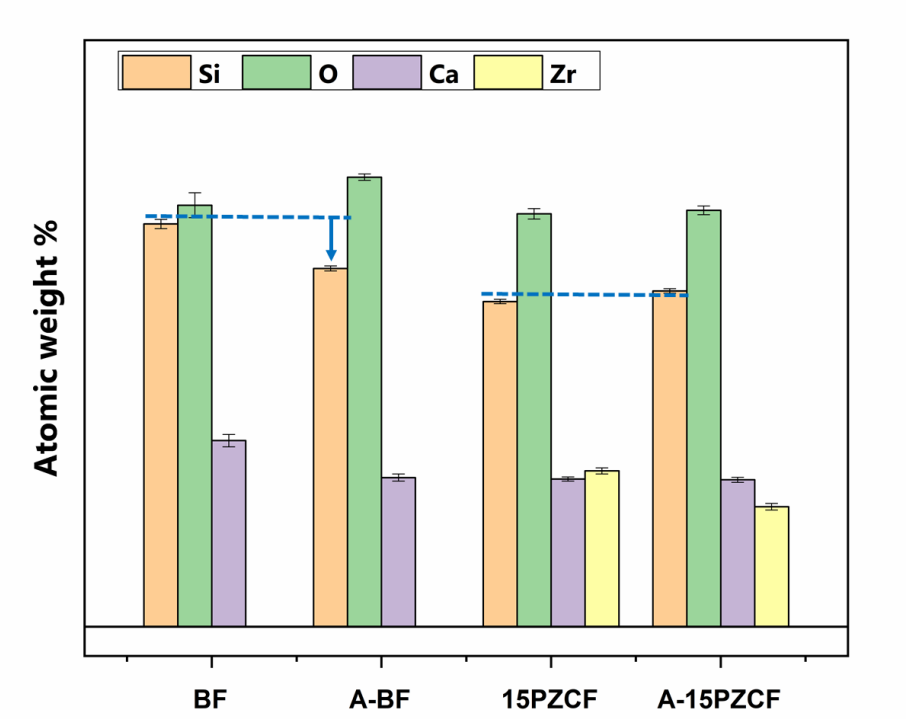

Figure 4.13: Atomic weight percentage of bare fiber (BF), aged bare fiber (A-BF), 15% ZrO_2 coated fiber (15PZCF), aged 15% ZrO_2 coated fiber (A-15PZCF). The standard error is shown as an error bar, and 10 measurements were made for every element.

of dwelling in the alkaline solutions. Additionally, the percentage of calcium (Ca) and oxygen (O) also remained the same. This means that the fibers coated with 15% ZrO_2 are providing protection to the attack of OH- ions of alkaline solutions. These findings indicated the nanoparticle coating of the E-glass fiber surface provides resistance against the alkaline condition. The lower reactivity of Zr-O bonds with OH- ions in the alkaline state allowed it to be chemically resistant [16, 96]. Moreover, the ZrO_2 nanoparticle protects itself from the attack of an alkaline environment via the formation thin hydrated layer on the fiber surface [108]. Furthermore, Si-O bonding on the glass fibers is about twice weaker than the Zr-O bonding due to the ionic nature of the bonding.

4.3 Conclusions

This chapter investigated the mechanical properties of E-glass fibers coated with SiO_2 and the chemical resistivity and mechanical characteristics of the ZrO_2 nanoparticles coated E-glass fibers. SEM micrographs of the fiber provide proof of nanoparticles' presence on the surface of the fibers. Firstly, dip-coating of amorphous SiO_2 nanoparticles on the E-glass fiber surface has adversely affected the mechanical properties of E-glass fibers. From the SEM micrograph, it can be concluded that this adverse effect occurred due to the fractured, non-homogeneous surface of the E-glass fibers after the coating. This may happen due to the amorphous phase of SiO_2 nanoparticles. Secondly, monoclinic ZrO_2 nanoparticles coating has been found to improve the tensile strength. ZrO_2 nanoparticle-coated fibers have a lower probability of failure at a specific stress over bare fibers of all concentrations, and coating can also improve the tensile strength of glass fibers. Additionally, ZrO_2 nanoparticle-coated fibers have been found to be resistant against highly alkaline solutions for four (04) days. From this chapter, it can be concluded that fibers coated with 15% ZrO_2 nanoparticles have the potential to withstand corrosion as well as the ability to improve the mechanical characteristics of E-glass fibers.

Chapter 5

Conclusions and Future Prospects

5.1 Conclusions and Future Work

Glass fibers are the most widely used reinforced materials in fiber-reinforced composites, and glass fibers supply the majority of the reinforcement materials. The property of the finished composites not only depends on the matrix material but also depends on reinforcement materials. Over the years, there have been published works in the literature about composites, but very few pieces of work focus only on the reinforcement material of single glass fibers. This thesis focuses on TiO_2, SiO_2, and ZrO_2, nanoparticles coating to study single E-glass fibers' mechanical and chemical properties. In the first study, TiO_2, nanoparticles in rutile phase of varied concentrations (5%, 10%, and 15%) were dip coated and chemically stabilized via the APTES solutions. After that, SEM, AFM, and XPS analysis proved the presence of nanoparticles as well as the chemical bonding of TiO_2, with APTES. Additionally, tensile tests were conducted on the nanoparticle-coated fibers and bare fibers to see the impact of TiO_2, nanoparticles concentrations on the mechanical property of E-glass fibers. After analyzing experimental data from the tensile tests following Weibull statistics, it was found

that all the concentration of TiO_2 nanoparticle-coated fibers are less likely to fail at a given stress than the bare fibers. Although the tensile strength has increased with all nanoparticle concentrations, fibers coated with 10% TiO_2, solution produced the greatest results. It was also concluded that the fracture surface's mirror region is correlated with the tensile strength of the glass fibers. The fibers with narrower mirror regions are expected to have a higher tensile strength.

In fourth chapter, the same coating technique had an adverse effect when amorphous SiO_2 nanoparticles were incorporated into the E-glass fibers. Fibers coated with nanoparticle solutions (5%, 10%, and 15% SiO_2) have decreased the glass fibers' tensile strength. SEM inspection of the fiber surface dip-coated with nanoparticles has found that SiO_2-coated fiber surface breaks just after coating and even before any annealing process. Further analysis of the surface have found that, amorphous SiO_2 nanoparticle coatings have formed a fractured surface and led to reduction of tensile strength on the glass fibers. The non-homogeneous nature of the fiber surface did not allow the stress to transfer along the fiber, instead accumulated the stress on the fiber imperfection region and ultimately led to the failure of glass fibers at lower stress. Additionally, the mechanical and chemical properties of the single E-glass fibers were investigated via the same dip-coating but for the monoclinic ZrO_2 nanoparticle solutions. Although the fiber was coated with different (5%, 10%, and 15% ZrO_2) concentrations of nanoparticle solutions, it was found that fibers that were coated with 15 ZrO_2 solutions were only capable of improving the corrosion resistance in highly alkaline solutions. Moreover, it was also found that 5% ZrO_2 coated fibers, and 10% ZrO_2 coated fibers are effective in enhancing the mechanical property of glass fibers even though they are not capable of providing resistance against the alkaline solution. These nanoparticle-coated fibers are expected to have superior mechanical and chemical properties in the composites.

Future work will be the first to see the effect of nanoparticle size and crystallinity on the mechanical and chemical properties of glass fibers. Besides, composites will be prepared using these nanoparticle-coated fibers, and this is expected to have superior mechanical and chemical properties.

Bibliography

[1] F. Aramide, P. Atanda, and O. Olorunniwo, "Mechanical properties of a polyester fibre glass composite," *International Journal of Composite Materials*, vol. 2, no. 6, pp. 147–151, 2012.

[2] H. Li, T. Charpentier, J. Du, and S. Vennam, "Composite reinforcement: Recent development of continuous glass fibers," *International Journal of Applied Glass Science*, vol. 8, no. 1, pp. 23–36, 2017.

[3] H. Li, P. Gu, J. Watson, and J. Meng, "Acid corrosion resistance and mechanism of e-glass fibers: boron factor," *Journal of Materials Science*, vol. 48, pp. 3075–3087, 2013.

[4] J. M. Stickel and M. Nagarajan, "Glass fiber-reinforced composites: from formulation to application," *International Journal of Applied Glass Science*, vol. 3, no. 2, pp. 122–136, 2012.

[5] M. Shioya and T. Kikutani, "Synthetic textile fibres: non-polymer fibres," in *Textiles and fashion*, pp. 139–155, Elsevier, 2015.

[6] F. T. Wallenberger, J. C. Watson, and H. Li, "Glass fibers," *Composites*, pp. 27–34, 2001.

[7] Z.-M. Huang, "Biocomposites," 2023.

[8] M. O. Seydibeyoglu, A. K. Mohanty, and M. Misra, *Fiber technology for fiber-reinforced composites*. Woodhead Publishing, 2017.

[9] R. A. Scott, *Textiles for protection*. Elsevier, 2005.

[10] J. Thomason, "Interfaces and interfacial effects in glass reinforced thermoplastics-keynote presentation," 2007.

[11] J. W. Hearle, *High-performance fibres*. Elsevier, 2001.

[12] B. Mahltig and Y. Kyosev, "Inorganic and composite fibers: production, properties, and applications," 2018.

[13] K. L. Loewenstein, "The manufacturing technology of continuous glass fibres," *(No Title)*, 1973.

[14] M. L. Korwin-Edson, D. A. Hofmann, and P. B. McGinnis, "Strength of high performance glass reinforcement fiber," *International journal of applied glass science*, vol. 3, no. 2, pp. 107–121, 2012.

[15] F. T. Wallenberger and P. A. Bingham, "Fiberglass and glass technology," *Energy-Friendly Compositions And Applications*, 2010.

[16] Y. V. Lipatov, S. Gutnikov, M. Manylov, and B. Lazoryak, "Effect of zro 2 on the alkali resistance and mechanical properties of basalt fibers," *Inorganic materials*, vol. 48, pp. 751–756, 2012.

[17] J. Thomason, *Glass fibre sizings: A review of the scientific literature*. Create Space Independent Publishing Platform, 2012.

[18] J. Thomason, *Glass fibre sizing: A review of size formulation patents*. Create Space Independent Publishing Platform, 2015.

[19] M. K. Ahmed, A. Bagheri Behboud, A. Kurucu, G. Kurt Çömlekçi, and M. Ordu, "Improved mechanical properties of the e-glass fibres through tio2 nanoparticle coating," *Materials Science and Technology*, pp. 1–9, 2023.

[20] J. L. Thomason, "Glass fibre sizing: A review," *Composites Part A: Applied Science and Manufacturing*, vol. 127, p. 105619, 2019.

[21] E. P. Plueddemann and E. P. Plueddemann, *Nature of adhesion through silane coupling agents*. Springer, 1991.

[22] J. Karger-Kocsis, H. Mahmood, and A. Pegoretti, "Recent advances in fiber/matrix interphase engineering for polymer composites," *Progress in Materials Science*, vol. 73, pp. 1–43, 2015.

[23] P. Zinck, E. Mäder, and J.-F. Gerard, "Role of silane coupling agent and polymeric film former for tailoring glass fiber sizings from tensile strength measurements," *Journal of materials science*, vol. 36, pp. 5245–5252, 2001.

[24] F. R. Jones, "Interphase in fiber-reinforced composites," *Wiley encyclopedia of composites*, pp. 1–6, 2011.

[25] M. Tanoglu, S. Ziaee, S. Mcknight, G. Palmese, and J. Gillespie, "Investigation of properties of fiber/matrix interphase formed due to the glass fiber sizings," *Journal of Materials Science*, vol. 36, pp. 3041–3053, 2001.

[26] Q. An, S. Tamrakar, J. W. Gillespie Jr, A. N. Rider, and E. T. Thostenson, "Tailored glass fiber interphases via electrophoretic deposition of carbon nanotubes: Fiber and interphase characterization," *Composites Science and Technology*, vol. 166, pp. 131–139, 2018.

[27] M. Tanoglu, S. H. McKnight, G. R. Palmese, and J. Gillespie Jr, "The effects of glass-fiber sizings on the strength and energy absorption of the fiber/matrix interphase under high loading rates," *Composites science and technology*, vol. 61, no. 2, pp. 205–220, 2001.

[28] R. Zhang, Y. Liu, Y. Huang, and L. Liu, "Effect of particle size and distribution of the sizing agent on the carbon fibers surface and interfacial shear strength (ifss) of its composites," *Applied surface science*, vol. 287, pp. 423–427, 2013.

[29] X. Gao, R. Jensen, S. McKnight, and J. Gillespie Jr, "Effect of colloidal silica on the strength and energy absorption of glass fiber/epoxy interphases," *Composites Part A: Applied Science and Manufacturing*, vol. 42, no. 11, pp. 1738–1747, 2011.

[30] Q. An and N. Andrew, "Rider, and erik t," *Thostenson." Hierarchical composite structures prepared by electrophoretic deposition of carbon nanotubes*

onto glass fibers." ACS applied materials & interfaces, vol. 5, pp. 2022–2032, 2013.

[31] Q. An, A. N. Rider, and E. T. Thostenson, "Electrophoretic deposition of carbon nanotubes onto carbon-fiber fabric for production of carbon/epoxy composites with improved mechanical properties," *Carbon*, vol. 50, no. 11, pp. 4130–4143, 2012.

[32] B. Fiedler, F. H. Gojny, M. H. G. Wichmann, W. Bauhofer, and K. Schulte, "Can carbon nanotubes be used to sense damage in composites?," in *Annales de Chimie: Science des Materiaux*, vol. 29, pp. 81–94, 2004.

[33] M. A. Alam and K. Al Riyami, "Shear strengthening of reinforced concrete beam using natural fibre reinforced polymer laminates," *Construction and Building Materials*, vol. 162, pp. 683–696, 2018.

[34] A. Warrier, A. Godara, O. Rochez, L. Mezzo, F. Luizi, L. Gorbatikh, S. V. Lomov, A. W. VanVuure, and I. Verpoest, "The effect of adding carbon nanotubes to glass/epoxy composites in the fibre sizing and/or the matrix," *Composites Part A: Applied Science and Manufacturing*, vol. 41, no. 4, pp. 532–538, 2010.

[35] H. Li, C. Richards, and J. Watson, "High-performance glass fiber development for composite applications," *International Journal of Applied Glass Science*, vol. 5, no. 1, pp. 65–81, 2014.

[36] F. T. Wallenberger, J. C. Watson, and H. Li, "Ppg industries, inc," *Glass Fibers, ASM Handbook*, vol. 21, 2001.

[37] R. Jindal, W. Jatmiko, I. V. Singh, R. Jayaganthan, *et al.*, "Elastic properties of clinopyroxene based glasses along diopside (camgsi 2 o 6)-jadeite (naalsi 2 o 6) join," *Journal of Minerals and Materials Characterization and Engineering*, vol. 11, no. 03, p. 267, 2012.

[38] S. Sundaram, *76th Conference on Glass Problems, Version A: A Collection of Papers Presented at the 76th Conference on Glass Problems, Greater Columbus Convention Center, Columbus, Ohio, November 2-5, 2015, Volume 37, Issue 1*, vol. 605. John Wiley & Sons, 2016.

[39] S. K. Lee and J. F. Stebbins, "The distribution of sodium ions in aluminosilicate glasses: a high-field na-23 mas and 3q mas nmr study," *Geochimica et Cosmochimica Acta*, vol. 67, no. 9, pp. 1699–1709, 2003.

[40] S. Wang and J. F. Stebbins, "Multiple-quantum magic-angle spinning 17o nmr studies of borate, borosilicate, and boroaluminate glasses," *Journal of the American Ceramic Society*, vol. 82, no. 6, pp. 1519–1528, 1999.

[41] H. Yamashita, K. Inoue, T. Nakajin, H. Inoue, and T. Maekawa, "Nuclear magnetic resonance studies of 0.139 mo (or m 2o)· 0.673 sio2·(0.188- x) al2o3· xb2o3 (m= mg, ca, sr and ba, m= na and k) glasses," *Journal of non-crystalline solids*, vol. 331, no. 1-3, pp. 128–136, 2003.

[42] L.-S. Du and J. F. Stebbins, "Network connectivity in aluminoborosilicate glasses: A high-resolution 11b, 27al and 17o nmr study," *Journal of Non-Crystalline Solids*, vol. 351, no. 43-45, pp. 3508–3520, 2005.

[43] L. Yang and J. Thomason, "The thermal behaviour of glass fibre investigated by thermomechanical analysis," *Journal of materials science*, vol. 48, pp. 5768–5775, 2013.

[44] G. Gavriliu, "Effects of added oxide and thermal history on young's modulus of added oxide (s)–na2o–sio2 glass," *Materials Letters*, vol. 48, no. 3-4, pp. 199–204, 2001.

[45] W. H. Otto, "Compaction effects in glass fibers," *Journal of the American Ceramic Society*, vol. 44, no. 2, pp. 68–72, 1961.

[46] Q. Zhong, D. Inniss, and C. R. Kurkjian, "Strength-flaw relationship of corroded pristine silica studied by atomic force microscopy," *MRS Online Proceedings Library (OPL)*, vol. 332, 1994.

[47] S. Kumarasamy, M. S. Z. Abidin, M. A. Bakar, M. Nazida, Z. Mustafa, and A. Anjang, "Effects of high and low temperature on the tensile strength of glass fiber reinforced polymer composites," in *IOP Conference Series: Materials Science and Engineering*, vol. 370, p. 012021, IOP Publishing, 2018.

[48] P. Bhawal, S. Ganguly, T. K. Das, S. Mondal, S. Choudhury, and N. Das, "Superior electromagnetic interference shielding effectiveness and electro-mechanical properties of ema-irgo nanocomposites through the in-situ reduction of go from melt blended ema-go composites," *Composites Part B: Engineering*, vol. 134, pp. 46–60, 2018.

[49] C. R. Kurkjian, P. Gupta, R. K. Brow, and N. Lower, "The intrinsic strength and fatigue of oxide glasses," *Journal of Non-Crystalline Solids*, vol. 316, no. 1, pp. 114–124, 2003.

[50] L. Yang and J. Thomason, "Effect of silane coupling agent on mechanical performance of glass fibre," *Journal of Materials Science*, vol. 48, pp. 1947–1954, 2013.

[51] W. Thomas, "An investigation of the factors affecting the strength of glass fiber," *Glass and Ceramics*, vol. 17, no. 10, pp. 549–550, 1960.

[52] D. B. Dingwell, "Redox viscometry of some fe-bearing silicate melts," *American Mineralogist*, vol. 76, no. 9-10, pp. 1560–1562, 1991.

[53] B. O. Mysen, "Redox equilibria and coordination of fe2+ and fe3+ in silicate glasses from 57fe mossbauer spectroscopy," *Journal of Non-Crystalline Solids*, vol. 95, pp. 247–254, 1987.

[54] C. L. McKinnis, "E-glass batch melting redox and its effect on specific glass properties," *Journal of Non-Crystalline Solids*, vol. 84, no. 1-3, pp. 381–389, 1986.

[55] M. D. Lund and Y. Yue, "Impact of drawing stress on the tensile strength of oxide glass fibers," *Journal of the American Ceramic Society*, vol. 93, no. 10, pp. 3236–3243, 2010.

[56] M. Lund and Y. Yue, *Tensile strength of glass fibers*. Faculty of Engineering and Science, Aalborg University, 2010.

[57] S. Freiman, "The fracture of glass: past, present, and future," *International Journal of Applied Glass Science*, vol. 3, no. 2, pp. 89–106, 2012.

[58] R. Gy, "Stress corrosion of silicate glass: a review," *Journal of non-crystalline solids*, vol. 316, no. 1, pp. 1–11, 2003.

[59] G. Bartenev, "The structure and strength of glass fibers of different chemical composition," *Materials Science and Engineering*, vol. 4, no. 1, pp. 22–28, 1969.

[60] A. G. Clare, P. F. Wachtel, and J. D. Musgraves, "Halide glasses," *Springer Handbook of Glass*, pp. 595–616, 2019.

[61] G. Quinn, "Nist recommended practice guide: fractography of ceramics and glasses, special publication (nist sp), national institue of standards and technology, gaiterhsburg, md," 2020.

[62] D. Uhlmann, *Elasticity and Strength in Glasses: Glass: Science and Technology*, vol. 5. Elsevier, 2012.

[63] K. K. Phani, "Strength distribution and gauge length extrapolations in glass fibre," *Journal of materials science*, vol. 23, pp. 1189–1194, 1988.

[64] P. Zinck, M. Pay, R. Rezakhanlou, and J. Gerard, "Mechanical characterisation of glass fibres as an indirect analysis of the effect of surface treatment," *Journal of Materials Science*, vol. 34, no. 9, pp. 2121–2133, 1999.

[65] B. Bergman, "On the estimation of the weibull modulus," *Journal of Materials Science Letters*, vol. 3, no. 8, pp. 689–692, 1984.

[66] M. K. Hossain, M. M. R. Chowdhury, M. B. Salam, J. Malone, M. V. Hosur, S. Jeelani, and N. W. Bolden, "Improved thermomechanical properties of carbon fiber reinforced epoxy composite using amino functionalized xdcnt," *Journal of Applied Polymer Science*, vol. 131, no. 17, 2014.

[67] D. Pedrazzoli, A. Pegoretti, and K. Kalaitzidou, "Synergistic effect of exfoliated graphite nanoplatelets and short glass fiber on the mechanical and interfacial properties of epoxy composites," *Composites Science and Technology*, vol. 98, pp. 15–21, 2014.

[68] A. Dorigato, S. Morandi, and A. Pegoretti, "Effect of nanoclay addition on the fiber/matrix adhesion in epoxy/glass composites," *Journal of Composite materials*, vol. 46, no. 12, pp. 1439–1451, 2012.

[69] C. Scheffler, S. Gao, R. Plonka, E. Mäder, S. Hempel, M. Butler, and V. Mechtcherine, "Interphase modification of alkali-resistant glass fibres and carbon fibres for textile reinforced concrete i: Fibre properties and durability," *Composites Science and Technology*, vol. 69, no. 3-4, pp. 531–538, 2009.

[70] Y. Dong, Y. Zhu, Y. Zhao, F. Liu, E. Wang, and Y. Fu, "Enhance interfacial properties of glass fiber/epoxy composites with environment-friendly water-based hybrid sizing agent," *Composites Part A: Applied Science and Manufacturing*, vol. 102, pp. 357–367, 2017.

[71] B. D. Jamnani, S. Hosseini, S. Rahmanian, S. A. Rashid, S. B. Mustapha, and S. K. Balavandy, "Grafting carbon nanotubes on glass fiber by dip coating technique to enhance tensile and interfacial shear strength," *Journal of Nanomaterials*, vol. 16, no. 1, pp. 306–306, 2016.

[72] A. Godara, L. Gorbatikh, G. Kalinka, A. Warrier, O. Rochez, L. Mezzo, F. Luizi, A. W. Van Vuure, S. V. Lomov, and I. Verpoest, "Interfacial shear strength of a glass fiber/epoxy bonding in composites modified with carbon nanotubes," *Composites Science and Technology*, vol. 70, no. 9, pp. 1346–1352, 2010.

[73] M. Reghat, A. Mirabedini, A. M. Tan, Y. Weizman, P. Middendorf, R. Bjekovic, L. Hyde, D. Antiohos, N. Hameed, F. K. Fuss, *et al.*, "Graphene as a piezo-resistive coating to enable strain monitoring in glass fiber composites," *Composites Science and Technology*, vol. 211, p. 108842, 2021.

[74] V. Prasad, K. Sekar, and M. Joseph, "Mechanical and water absorption properties of nano tio2 coated flax fibre epoxy composites," *Construction and Building Materials*, vol. 284, p. 122803, 2021.

[75] V. Prasad, K. Sekar, S. Varghese, and M. Joseph, "Evaluation of interlaminar fracture toughness and dynamic mechanical properties of nano tio2 coated flax fibre epoxy composites," *Polymer Testing*, vol. 91, p. 106784, 2020.

[76] V. Prasad, C. Muhammed Hunize, R. Abhiraj, M. Jospeh, K. Sekar, and M. Ali, "Mechanical properties of flax fiber reinforced composites manufactured using hand layup and compression molding—a comparison," in *Advances in Industrial and Production Engineering: Select Proceedings of FLAME 2018*, pp. 781–789, Springer, 2019.

[77] V. Prasad, M. Joseph, and K. Sekar, "Investigation of mechanical, thermal and water absorption properties of flax fibre reinforced epoxy composite with nano tio2 addition," *Composites part A: Applied science and manufacturing*, vol. 115, pp. 360–370, 2018.

[78] A. Ajith, G. Xian, H. Li, Z. Sherief, and S. Thomas, "Surface grafting of flax fibres with hydrous zirconia nanoparticles and the effects on the tensile and bonding properties," *Journal of Composite Materials*, vol. 50, no. 5, pp. 627–635, 2016.

[79] U. Nagel, L. Yang, C. Kao, and J. Thomason, "Effects of thermal recycling temperatures on the reinforcement potential of glass fibers," *Polymer Composites*, vol. 39, no. 4, pp. 1032–1040, 2018.

[80] V. Rybin, Utkin, and N. Baklanova, "Alkali resistance, microstructural and mechanical performance of zirconia-coated basalt fibers," *Cement and Concrete Research*, vol. 53, pp. 1–8, 2013.

[81] K. W. Shinato, F. Huang, and Y. Jin, "Principle and application of atomic force microscopy (afm) for nanoscale investigation of metal corrosion," *Corrosion Reviews*, vol. 38, no. 5, pp. 423–432, 2020.

[82] V. Bellitto, *Atomic force microscopy: imaging, measuring and manipulating surfaces at the atomic scale*. BoD–Books on Demand, 2012.

[83] P. Harinath, N. Radadia, S. Bramhe, D. Surendran, V. Sabane, A. Singh, T. N. Kim, R. Sharbidre, B. J. Cheol, L. Peters, *et al.*, "Analysis of microstructural, thermal and mechanical properties of unidirectional glass fiber fabrics exhibiting sizing migration," *Composites Part B: Engineering*, vol. 164, pp. 570–575, 2019.

[84] E. Jalali, S. Maghsoudi, and E. Noroozian, "A novel method for biosynthesis of different polymorphs of tio2 nanoparticles as a protector for bacillus thuringiensis from ultra violet," *Scientific Reports*, vol. 10, no. 1, p. 426, 2020.

[85] G. Duoerkun, Y. Zhang, Z. Shi, X. Shen, W. Cao, T. Liu, J. Liu, Q. Chen, and L. Zhang, "Construction of n-tio 2/p-ag 2 o junction on carbon fiber cloth with vis–nir photoresponse as a filter-membrane-shaped photocatalyst," *Advanced Fiber Materials*, vol. 2, pp. 13–23, 2020.

[86] B. Erdem, R. A. Hunsicker, G. W. Simmons, E. D. Sudol, V. L. Dimonie, and M. S. El-Aasser, "Xps and ftir surface characterization of tio2 particles used in polymer encapsulation," *Langmuir*, vol. 17, no. 9, pp. 2664–2669, 2001.

[87] G. Liu, W. Jaegermann, J. He, V. Sundström, and L. Sun, "Xps and ups characterization of the tio2/znpcgly heterointerface: alignment of energy levels," *The Journal of Physical Chemistry B*, vol. 106, no. 23, pp. 5814–5819, 2002.

[88] F. A. Stevie and C. L. Donley, "Introduction to x-ray photoelectron spectroscopy," *Journal of Vacuum Science & Technology A*, vol. 38, no. 6, 2020.

[89] D. Briggs, "Handbook of x-ray photoelectron spectroscopy cd wanger, wm riggs, le davis, jf moulder and ge muilenberg perkin-elmer corp., physical electronics division, eden prairie, minnesota, usa, 1979. 190 pp. 195,$''$ $Surface and Interface Analysis, vol.\ 3, no.\ 4, pp.\ v - -v, 1981.$

[90] M. D. Lund and Y. Yue, "Fractography and tensile strength of glass wool fibres," *Journal of the Ceramic Society of Japan*, vol. 116, no. 1356, pp. 841–845, 2008.

[91] M. Zhangwei, W. Zhifeng, L. Huanhuan, P. Fufei, C. Zhenyi, and W. Tianxing, "Tensile strength and failure behavior of bare mode fibers," *Optical Fiber Tecnology*, vol. 52, p. 1, 2019.

[92] S. Semjonov and C. Kurkjian, "Strength of silica optical fibers with micron size flaws," *Journal of non-crystalline solids*, vol. 283, no. 1-3, pp. 220–224, 2001.

[93] F. Ellyin and R. Maser, "Environmental effects on the mechanical properties of glass-fiber epoxy composite tubular specimens," *Composites Science and Technology*, vol. 64, no. 12, pp. 1863–1874, 2004.

[94] U. Magarajan, D. Arvind, N. Kannan, P. Hemanandan, *et al.*, "A comparative study on the static mechanical properties of glass fibre vs glass-jute fibre polymer composite," *Materials Today: Proceedings*, vol. 5, no. 2, pp. 6711–6716, 2018.

[95] M. Aslan, M. Tufan, and T. Küçükömeroğlu, "Tribological and mechanical performance of sisal-filled waste carbon and glass fibre hybrid composites," *Composites Part B: Engineering*, vol. 140, pp. 241–249, 2018.

[96] C. Scheffler, T. Förster, E. Mäder, G. Heinrich, S. Hempel, and V. Mechtcherine, "Aging of alkali-resistant glass and basalt fibers in alkaline solutions: Evaluation of the failure stress by weibull distribution function," *Journal of Non-Crystalline Solids*, vol. 355, no. 52-54, pp. 2588–2595, 2009.

[97] A. Chira, A. Kumar, T. Vlach, L. Laiblová, A. S. Škapin, and P. Hájek, "Property improvements of alkali resistant glass fibres/epoxy composite with nanosilica for textile reinforced concrete applications," *Materials & Design*, vol. 89, pp. 146–155, 2016.

[98] E. Martynova and H. Cebulla, "Glass fibers," *Inorganic and composite fibers*, pp. 131–163, 2018.

[99] Y. V. Lipatov, S. Gutnikov, M. Manylov, E. Zhukovskaya, and B. Lazoryak, "High alkali-resistant basalt fiber for reinforcing concrete," *Materials & Design*, vol. 73, pp. 60–66, 2015.

[100] Q. Zhang, S. Li, S. Gong, G. Zhang, G. Xi, and Y. Wu, "Study on flexural properties of basalt fiber textile reinforced concrete (btrc) sheets including short ar-glass fibers," *Frontiers in Materials*, vol. 7, p. 277, 2020.

[101] C.-D. Li, Z.-C. Duan, Q. Chen, Z.-F. Chen, F. E. Boafo, W.-P. Wu, and J.-M. Zhou, "The effect of drying condition of glassfibre core material on the thermal conductivity of vacuum insulation panel," *Materials & Design*, vol. 50, pp. 1030–1037, 2013.

[102] E. De la Rosa-Cruz, L. Diaz-Torres, P. Salas, V. Castano, and J. Hernandez, "Evidence of non-radiative energy transfer from the host to the active ions in monoclinic zro2: Sm3+," *Journal of Physics D: Applied Physics*, vol. 34, no. 14, p. L83, 2001.

[103] O. Mangla and S. Roy, "Monoclinic zirconium oxide nanostructures having tunable band gap synthesized under extremely non-equilibrium plasma conditions," *Multidisciplinary Digital Publishing Institute Proceedings*, vol. 3, no. 1, p. 10, 2018.

[104] S. Thakur, S. Sareen, M. Verma, K. Kaur, and V. Mutreja, "Synthesis of elusive monoclinic zro2 nanostructures via hydrothermal treatment," *Journal of Inorganic and Organometallic Polymers and Materials*, pp. 1–18, 2023.

[105] N. Baklanova and A. Utkin, "Alkali resistance, improved alkali resistance of basalt fibers with zirconia and titania coatings," *Cem. Concr. Res.*, vol. 53, pp. 1–8, 2013.

[106] N. Baklanova, O. Kiselyova, A. Titov, and T. Zima, "Microstructural features of the zro2 interfacial coatings on sic fibers before and after exposition to air at high temperatures," *Journal of the European Ceramic Society*, vol. 28, no. 8, pp. 1687–1696, 2008.

[107] A. Bahari, M. Ghovati, and A. Hashemi, "Studying of sio 2/capron nanocomposite as a gate dielectric film for improved threshold voltage," *Applied Physics A*, vol. 125, pp. 1–7, 2019.

[108] A. Paul, "Chemical durability of glasses; a thermodynamic approach," *Journal of materials science*, vol. 12, pp. 2246–2268, 1977.

[109] M. Zhang and J. P. Matinlinna, "E-glass fiber reinforced composites in dental applications," *Silicon*, vol. 4, pp. 73–78, 2012.